

Spatial Variability in the Ratio of Interstellar Atomic Deuterium to Hydrogen. II. Observations toward γ^2 Velorum and ζ Puppis by the Interstellar Medium Absorption Profile Spectrograph¹

George Sonneborn,^{2,3} Todd M. Tripp,⁴ Roger Ferlet,^{3,5} Edward B. Jenkins,⁴ U. J. Sofia,⁶ Alfred Vidal-Madjar,^{3,5} and Przemysław R. Woźniak⁴

ABSTRACT

High resolution far ultraviolet spectra of the early-type stars γ^2 Vel and ζ Pup were obtained to measure the interstellar deuterium abundances in these directions. The observations were made with the Interstellar Medium Absorption Profile Spectrograph (IMAPS) during the *ORFEUS-SPAS II* mission in 1996. IMAPS spectra cover the wavelength range 930–1150Å with $\lambda/\Delta\lambda \sim 80,000$. The interstellar D I features are resolved and cleanly separated from interstellar H I in the Ly δ and Ly ϵ profiles of both sight lines, and also in the Ly γ profile of ζ Pup. The D I profiles were modeled using a velocity template derived from several N I lines in the IMAPS spectra recorded at higher signal-to-noise. To find the best D I column density, we minimized χ^2 for model D I profiles that included not only the $N(\text{D I})$ as a free parameter, but also the effects of several potential sources of systematic error which were allowed to vary as free parameters. H I column densities were measured by analyzing Ly α absorption profiles in a large number of *IUE* high dispersion spectra for each of these stars and applying this same χ^2 -minimization technique. Ultimately we found that $\text{D/H} = 2.18_{-0.31}^{+0.36} \times 10^{-5}$ for γ^2 Vel and $1.42_{-0.23}^{+0.25} \times 10^{-5}$ for ζ Pup, values that contrast markedly with D/H derived in Paper I for δ Ori A (the stated errors are 90% confidence limits). Evidently, the atomic D/H ratio in the ISM, averaged over path lengths of 250 to 500 pc, exhibits significant spatial variability. Furthermore, the observed spatial variations in D/H do not appear to be anticorrelated with N/H, one measure

¹This paper is dedicated in memory of Judith L. Tokel, wife of the first author, who passed away on 2000 June 10. Her enthusiastic support and encouragement were essential to its successful completion.

²Laboratory for Astronomy and Solar Physics, Code 681, NASA Goddard Space Flight Center, Greenbelt, MD 20771; george.sonneborn@gsfc.nasa.gov

³Guest Investigator with the IMAPS instrument on the *ORFEUS-SPAS II* mission

⁴Princeton University Observatory, Princeton, NJ 08544; tripp@astro.princeton.edu, ebj@astro.princeton.edu, woźniak@astro.princeton.edu

⁵Institut d’Astrophysique de Paris, 98bis Blvd. Arago, 75014 Paris, France; ferlet@iap.fr, alfred@iap.fr

⁶Dept. of Astronomy, Whitman College, 345 Boyer Ave., Walla Walla, WA 99362; sofiauj@whitman.edu

of heavy element abundances. We briefly discuss some hypotheses to explain the D/H spatial variability. Within the framework of standard Big Bang Nucleosynthesis, the large value of D/H found toward γ^2 Vel is equivalent to a cosmic baryon density of $\Omega_B h^2 = 0.023 \pm 0.002$, which we regard as an upper limit since there is no correction for the destruction of deuterium in stars.

Subject headings: ISM: Abundances — Cosmology: Observations — ISM: Evolution — Ultraviolet: ISM — Stars: Individual (γ^2 Vel, ζ Pup)

1. INTRODUCTION

The abundance ratio of atomic deuterium to hydrogen (D/H) in interstellar gas is widely regarded as an important tracer of galactic chemical evolution (Audouze & Tinsley 1974; Boesgaard & Steigman 1985; Tosi et al. 1998) and a key discriminant of the cosmic baryon-to-photon ratio (η) in Big Bang Nucleosynthesis (BBN, Walker et al. 1991). A standard interpretation is that D should not be produced in significant quantities in astrophysical sites other than the Big Bang (Epstein, Latimer, & Schramm 1976). The generally accepted viewpoint is that while D is produced primordially, its destruction takes place when some of the gas is cycled through stars. The uncertainties surrounding this process represent a stumbling block in arriving at the primordial value. For this reason, a measurement of D/H is often regarded as a lower limit to the primordial ratio, and this may be translated into an upper limit to η (for BBN, larger D/H implies lower η).

Rogerson & York (1973) made the first measurement of the atomic D/H abundance ratio in the interstellar medium (ISM) on the line of sight toward β Cen. Measurements with the *Copernicus* satellite toward an additional 14 stars ($100 < d < 500$ pc) found that D/H values cluster around 1.5×10^{-5} , but with a dispersion that, in some cases, seemed to exceed the stated uncertainties (see review by Vidal-Madjar & Gry 1984). While a simple interpretation of the *Copernicus* data suggested that the D/H measurements revealed spatial variations, the reality of these differences has been difficult to substantiate due to concerns stemming from the somewhat inadequate resolution of *Copernicus* (15 km s^{-1} FWHM) for this purpose.

Using the Goddard High Resolution Spectrograph (GHRS) and Space Telescope Imaging Spectrograph (STIS) on the *Hubble Space Telescope* (*HST*), several measurements of D/H in the local interstellar medium (LISM, $d < 100$ pc) have been made with observations of Ly α (see Lemoine et al. 1999 for a review). Linsky et al. (1993, 1995) found $\text{D/H} = 1.60_{-0.19}^{+0.14} \times 10^{-5}$ toward Capella. Vidal-Madjar et al. (1998) reported evidence for a factor of ~ 2 difference in D/H between two components on the line of sight toward the white dwarf G191-B2B ($d = 75$ pc). Sahu et al. (1999) re-evaluated the GHRS data as well as new STIS echelle spectra of G191-B2B and concluded that, as a result of improved instrumental characterization (echelle scattered light

correction near Ly α), D/H values in both components appeared to be consistent with the usual LISM value. Questions remain, however. For example, Howk & Sembach (2000) found a different STIS echelle scattered light correction, one that agrees with the GHRS Ly α profile (Vidal-Madjar 2000). The resolution of the conflicting conclusions about the G191-B2B sightline may be provided by observations of higher Lyman series lines (Ly β and Ly γ) by the *Far Ultraviolet Spectroscopic Explorer* (*FUSE*, Moos et al. 2000).

The Interstellar Medium Absorption Profile Spectrograph (IMAPS) provides a new window to study deuterium in the Galaxy by virtue of its wavelength coverage and very high spectral resolution ($\lambda/\Delta\lambda \sim 80,000$) which alleviate many of the previous obstacles to accurate D/H measurements. Prior to the IMAPS deuterium studies, D/H measurements in our galaxy after the *Copernicus* mission have been confined to the local ISM, since the saturated core of H I Ly α envelopes the D I Ly α feature for $N(\text{H I}) \gtrsim 1 \times 10^{19} \text{ cm}^{-2}$ and higher Lyman lines lie beyond the reach of *HST*. The goal of the IMAPS deuterium program is to obtain high-quality measurements of D/H on sightlines toward bright OB stars beyond the LISM. In the first paper of this series, Jenkins et al. (1999a, hereafter Paper I) measured the D/H abundance ratio toward δ Ori A using IMAPS spectra. They found $\text{D/H} = 0.74_{-0.13}^{+0.19} \times 10^{-5}$, a value that is much lower than that found in the LISM. Paper I also showed that the low abundance of D toward δ Ori A is *not* accompanied by an overabundance of N and O relative to H, as would be expected if the gas had been more thoroughly cycled through stellar interiors. We note that two other deuterium measurements using the Tübingen echelle spectrograph (resolution $\lambda/\Delta\lambda \sim 10,000$) on the *ORFEUS-SPAS II* mission have been recently reported: Gözl et al. (1998) found $\text{D/H} = 0.8_{-0.4}^{+0.7} \times 10^{-5}$ toward BD +28° 4211, an O-type subdwarf ~ 100 pc away, and Bluhm et al. (1999) measured $\text{D/H} = 1.2_{-0.4}^{+0.5} \times 10^{-5}$ toward BD +39° 3226, a sdO star located ~ 270 pc from the Sun.

In this paper we analyze the lines of sight toward two well-known hot stars, γ^2 Velorum (HD 68273) and ζ Puppis (HD 66811). They are among the brightest stars in the sky at 1000 Å, well studied by *Copernicus*, have H I column densities $\lesssim 10^{20} \text{ cm}^{-2}$, and hence are prime D/H targets for IMAPS. These stars were observed under an *ORFEUS-SPAS II* Guest Investigator program.

Table 1. Stellar data

Name	HD	l^{II}	b^{II}	Spectral Type	V (mag)	$v \sin i$ (km s ⁻¹)	Δv_{LSR}^a (km s ⁻¹)	d^b (pc)
ζ Pup	66811	253°98	-4°71	O5 Iaf	2.25	211	-18.04	429 ⁺¹²⁰ ₋₇₇
γ^2 Vel	68273	262°81	-7°70	WC8+O8	1.78	...	-17.48	258 ⁺⁴¹ ₋₃₁

^a $v_{LSR} = v_{helio} + \Delta v_{LSR}$

^bSchaerer et al. (1997)

The sightlines to γ^2 Vel and ζ Pup have been studied extensively (γ^2 Vel: Morton & Bhavsar 1979; Sahu 1992; Fitzpatrick & Spitzer 1994; ζ Pup: Morton & Dinerstein 1976; Morton 1978), including D/H measurements with observations from the *Copernicus* satellite. York & Rogerson (1976) found $D/H = 2.0_{-0.7}^{+1.1} \times 10^{-5}$ toward γ^2 Vel. Vidal-Madjar et al. (1977) studied the sightline toward ζ Pup and found that solutions consistent with the data permit a wide range of D/H values ($1.7 \times 10^{-5} \lesssim D/H \lesssim 2.5 \times 10^{-4}$). γ^2 Vel and ζ Pup are the most luminous stars in the Vela-Puppis region. Their role in powering the Gum Nebula and their relationship to the Vela OB2 association, Vela supernova remnants, and various structures in the ISM in Vela-Puppis have been analyzed by Sahu (1992). Table 1 summarizes some basic properties of the two stars. The distances listed were derived from *HIPPARCOS* data by Schaerer, Schmutz & Grenon (1997), placing γ^2 Vel significantly closer than earlier estimates.

γ^2 Vel is the closest (and brightest) Wolf-Rayet star and consequently it has been studied intensively for more than a century (van der Hucht et al. 1981). Nevertheless, due to the complexity of the stellar system, its fundamental stellar parameters have been continuously debated and revised (as recently as 1997 when several papers were published, e.g., Schaerer et al. 1997; Schmutz et al. 1997). γ^2 Vel is a double-lined spectroscopic binary star composed of a WR star (WC8) and a late O star (O8 III) of comparable brightness. The complex properties of this system are evident in the significant changes in the UV spectrum, and this behavior will be addressed in §4.3 when we discuss our determination of the interstellar hydrogen column density through measurements of the Ly α absorption feature.

ζ Pup is an extremely luminous, massive star (O4 Iaf) and the brightest O-type star in the sky. It is a prototype for O-star spectral properties and variability (Morton & Underhill 1977; Massa et al. 1995) and theoretical understanding of radiation-driven winds in massive stars (e.g. Puldrach et al. 1994). ζ Pup is believed to be a single star.

The high velocity resolution provided by IMAPS opens the way for more accurate line profile measurements in the far ultraviolet spectra of bright stars. Our observations of γ^2 Vel and ζ Pup described in §2 build on our earlier results for δ Ori A described in Paper I. We follow with discussions of how we derived D I column densities (§3), H I column densities (§4), and values for D/H and N/H (§5). The paper concludes with a discussion in §6 of the possible implications of the differences in D/H for the three stars covered in this paper and Paper I.

2. OBSERVATIONS

The spectra analyzed in this paper were obtained with IMAPS during the *ORFEUS-SPAS II* mission (STS-80) in late 1996 (see Hurwitz et al. 1998). The design of IMAPS and its performance on earlier flights have been described in detail by Jenkins et al. (1988, 1996). In Paper I we described the in-flight performance of IMAPS during the 1996 mission. Here we only summarize the instrument’s principal characteristics.

IMAPS is an objective-grating echelle spectrograph designed to record the far-UV spectrum of bright stars at high spectral resolution. The optical design consists of a wire grid collimator to reject off-axis light from stars other than the target, an echelle grating with a 63° blaze angle, and a parabolic cross disperser. The spectral format is imaged on a solid KBr photocathode, whose electrons are magnetically focussed on a windowless, back-illuminated CCD with a 320x256 pixel format. The nominal wavelength range of 930–1150 Å is obtained in four selectable tilts that span the free spectral range of the echelle grating. The gratings were coated with LiF over aluminum, providing excellent throughput longward of 1000 Å. Although the reflectivity of LiF drops substantially shortward of 1000 Å, IMAPS achieved a useful throughput even in the 930 – 980 Å region. The spectral resolution in IMAPS spectra obtained during the 1996 flight was approximately $\lambda/\Delta\lambda \sim 80,000$, or $\leq 4 \text{ km s}^{-1}$. The telluric O I lines (e.g. $\lambda 950.112$ near Ly δ - see Fig 1) have FWHM $\sim 5 \text{ km s}^{-1}$, but these lines are probably partly resolved in IMAPS spectra (see Jenkins et al. 1999b).

γ^2 Vel and ζ Pup were chosen for this IMAPS Guest Investigator program because they were available in 1996 November, have a flux near Ly δ $> 10^{-9} \text{ erg cm}^{-2} \text{ s}^{-1} \text{ \AA}^{-1}$, have $v \sin i \gtrsim 100 \text{ km s}^{-1}$, and $N(\text{H I}) \lesssim 10^{20} \text{ cm}^{-2}$.

γ^2 Vel was observed by IMAPS on 1996 November 27 14:34–15:11 and 16:00–16:47 UT for a total of 4224 s. ζ Pup was observed on 1996 November 26 18:44–19:23 and 20:16–20:57 UT also for a total of 4224 s. The exposure time at each echelle grating position ranged from 817.6 s to 1226.4 s. These exposure times were chosen to obtain spectra with good signal-to-noise (S/N) ratios near the cores of the D I Ly δ (949.485 Å) and Ly ϵ (937.548 Å) lines. Typically, we found S/N=10–15 in the local continuum near the Ly δ and Ly ϵ interstellar features.

3. COLUMN DENSITY OF ATOMIC DEUTERIUM

3.1. General Considerations

The data reduction and analysis of the γ^2 Vel and ζ Pup spectra and the determination of the D I column densities were identical to those described in Paper I for the line of sight toward δ Ori A. IMAPS spectra were analyzed to determine the total $N(\text{D I})$ (§3.3 and §3.4). A large number of *International Ultraviolet Explorer (IUE)* high resolution Ly α spectra were obtained from the National Space Science Data Center archive to determine the total H I column density ($N(\text{H I})$) in §4. We note that given that $N(\text{H I}) \sim 10^{20} \text{ cm}^{-2}$ on these sightlines and that D/H $\sim 10^{-5}$, the gas that gives rise to the H I Ly α damping wings is the same gas responsible for the D I Ly δ and Ly ϵ features.

In §3.2 we show that N I is a good tracer of H I and D I on these sight lines. The line of sight column density per unit velocity [$N_a(v)$, see Paper I] for N I, defined by a range of N I lines recorded in the IMAPS spectra, provided a velocity template for modelling the D I profiles. The

high S/N for the N I lines helped to constrain the model profiles that gave an acceptable fit to the lower S/N D I lines. This can prevent noise in the D I profiles from giving arbitrarily large or small $N(\text{D I})$ at specific velocities. We did not decompose the velocity profiles of N I or D I into separate (blended) Gaussian components – the D/H ratios determined here were based on total column densities for each sight line.

Using the method outlined in Paper I, we corrected for the effects of the weak lines Fe II $\lambda 937.652$ and H₂ Lyman 14–0 $P(2)$ $\lambda 949.351$. The Fe II line is located at +51 km s⁻¹ in γ^2 Vel and at +53 km s⁻¹ in ζ Pup on the heliocentric velocity scale whose zero point is the laboratory wavelength of D I Ly ϵ (see Figs. 1 and 2). The H₂ line is located at +10 km s⁻¹ in γ^2 Vel and at +12 km s⁻¹ in ζ Pup on the D I Ly δ heliocentric velocity scale. The strength and shape of these features were computed from other transitions of the same species recorded at longer wavelengths (and higher S/N) in the IMAPS spectra of γ^2 Vel and ζ Pup. The computed central residual intensities of these features are nearly identical for the two stars: 0.66 for Fe II $\lambda 937.6$ and 0.95 for H₂ $\lambda 949.3$. The other potentially contaminating lines noted in Table 1 of Paper I can safely be ignored.

The possible contamination of the Ly δ order by scattered light from an adjacent order that contains the strong absorption lines of the N I $\lambda\lambda 954$ multiplet was evaluated in the same manner as described in Paper I. The χ^2 analysis found that any residual contamination of the spectrum in the vicinity of Ly δ by the pattern of saturated N I features was < 1% of the continuum in both γ^2 Vel and ζ Pup. Amplitudes for this correction larger than $\sim 1\%$ caused unacceptably bad deviations in the bottom of the H I Ly δ profile. Given the general noise characteristics of the Ly δ profiles, this is a negligible effect.

For the case of γ^2 Vel, there is another potential contamination source. A companion star, γ^1 Vel, is located 42'' to the southwest of γ^2 Vel. Its light should be accepted along with that from γ^2 Vel, since IMAPS is an objective-grating spectrograph without an entrance slit to reject unwanted sources. (The grid collimator rejects light coming from more than 1° from the axis, however.) γ^1 Vel is 2.5 magnitudes fainter than γ^2 Vel in V and has a spectral classification of B1 IV (Hoffleit & Jaschek, 1982). Even though γ^1 Vel is cooler than γ^2 Vel, its flux is not diminished much below the peak of the Planck distribution at our wavelengths of interest, so we expect its intensity at a given wavelength to be not more than about a factor of 10 fainter than γ^2 Vel. Fortunately, when the observations were taken the roll angle of the spacecraft about the optical axis of IMAPS (governed by the position of the Sun in the sky) was such that the faint spectrum of γ^1 Vel was displaced along the cross dispersion direction toward the long-wavelength part of the format. As a consequence, any spectral segment in the spectrum of γ^2 Vel had light superposed on it from shorter wavelengths in γ^1 Vel (the separation was slightly less than the distance between 3 echelle orders). The rapid decline in the sensitivity of IMAPS toward shorter wavelengths thus amplified the factor of 10 disparity in relative fluxes at any given position on the format. Therefore, the contamination of the γ^2 Vel spectrum by light from γ^1 Vel is negligible. As a final note, on visual inspection we are unable to see any ghost-like spectrum of γ^1 Vel on top of

the spectrum of γ^2 Vel.

The Lyman line profiles for γ^2 Vel and ζ Pup are shown in Figures 1 and 2. These profiles have been corrected for Fe II and H₂ line absorption, as described above. The background levels near the D I lines were determined from the broad, saturated cores of the adjacent H I profiles. As explained in Paper I, we compared resolution-degraded forms of the IMAPS profiles with those recorded by *Copernicus* to test the proposition that the cores of the H I lines indeed represented the zero-intensity levels in the vicinity of the adjacent D I features. This was done to check that we were not being misled by an effect from possible strong, broad wings extending away from the main peak in the instrumental profile of IMAPS. We concluded that indeed the cores of the H I profiles provided very good estimates of the zero levels in the vicinity of the D I lines.

The best answers for $N(\text{D I})$ and the deviations permitted by the data were evaluated by minimizing χ^2 (see Lampton, Margon & Bowyer 1976 and Bevington & Robinson 1992 for details) when all of our unknown parameters were allowed to vary. The ten free parameters for γ^2 Vel are (1) $N(\text{D I})$, (2) the gas temperature T , (3-8) the continuum slopes, Y-intercepts, and background levels for Ly δ and Ly ϵ , (9) a shift in the velocity zero point between the D I lines and the N I template, and (10) a coefficient for scaling the N I contamination signal in Ly δ (see §3.2 in Paper I). The gas temperature is an important parameter because the D I line can be broadened significantly compared to the N I template by thermal motions; see §4.1 in Paper I for details. There are three additional free parameters for ζ Pup because of the addition of Ly γ to the analysis. Note that the linear continuum fitting (with specific velocity limits as given in §§3.3 and 3.4) is an integral part of the χ^2 evaluation, i.e., the deviations of the continuum levels are considered, in addition to the behavior inside the D I profiles. The same holds for the zero level as defined by the bottom of the adjacent H I profile. We used Powell’s method (Press et al. 1992, p. 406) to find the minimum χ^2 . We then set confidence limits by increasing (or decreasing) $N(\text{D I})$ and T with the other parameters freely varying until χ^2 increased by the appropriate amount for the confidence limit of interest with two useful parameters, $N(\text{D I})$ and T . We also used different initial values to establish that the minimum χ^2 is unique.

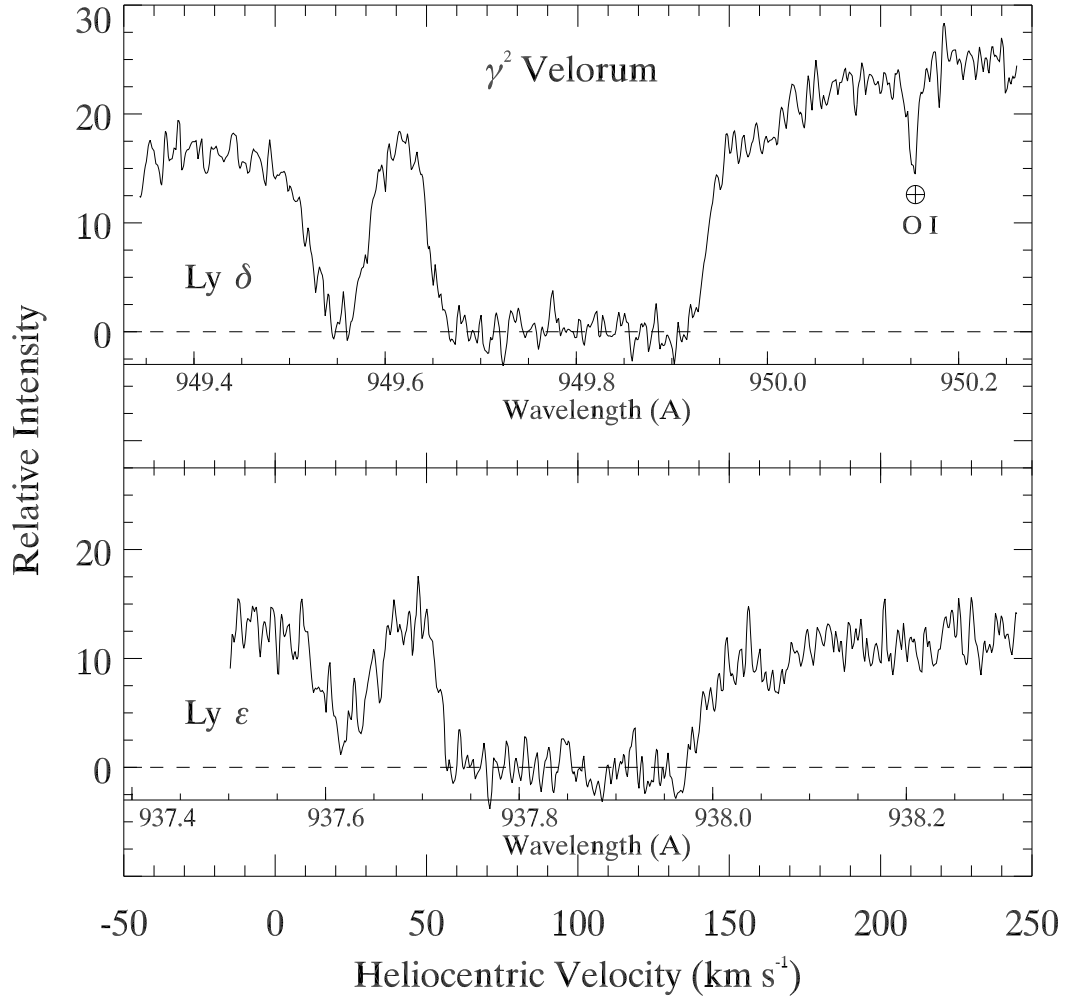


Fig. 1.— Line profiles of Ly δ and Ly ϵ from IMAPS spectra for γ^2 Vel. The zero-point of the velocity scale is computed with respect to the laboratory wavelengths of the D I lines. The narrow width of O I* λ 950.112 telluric line indicates the spectral resolution is $\lambda/\Delta\lambda \sim 80,000$.

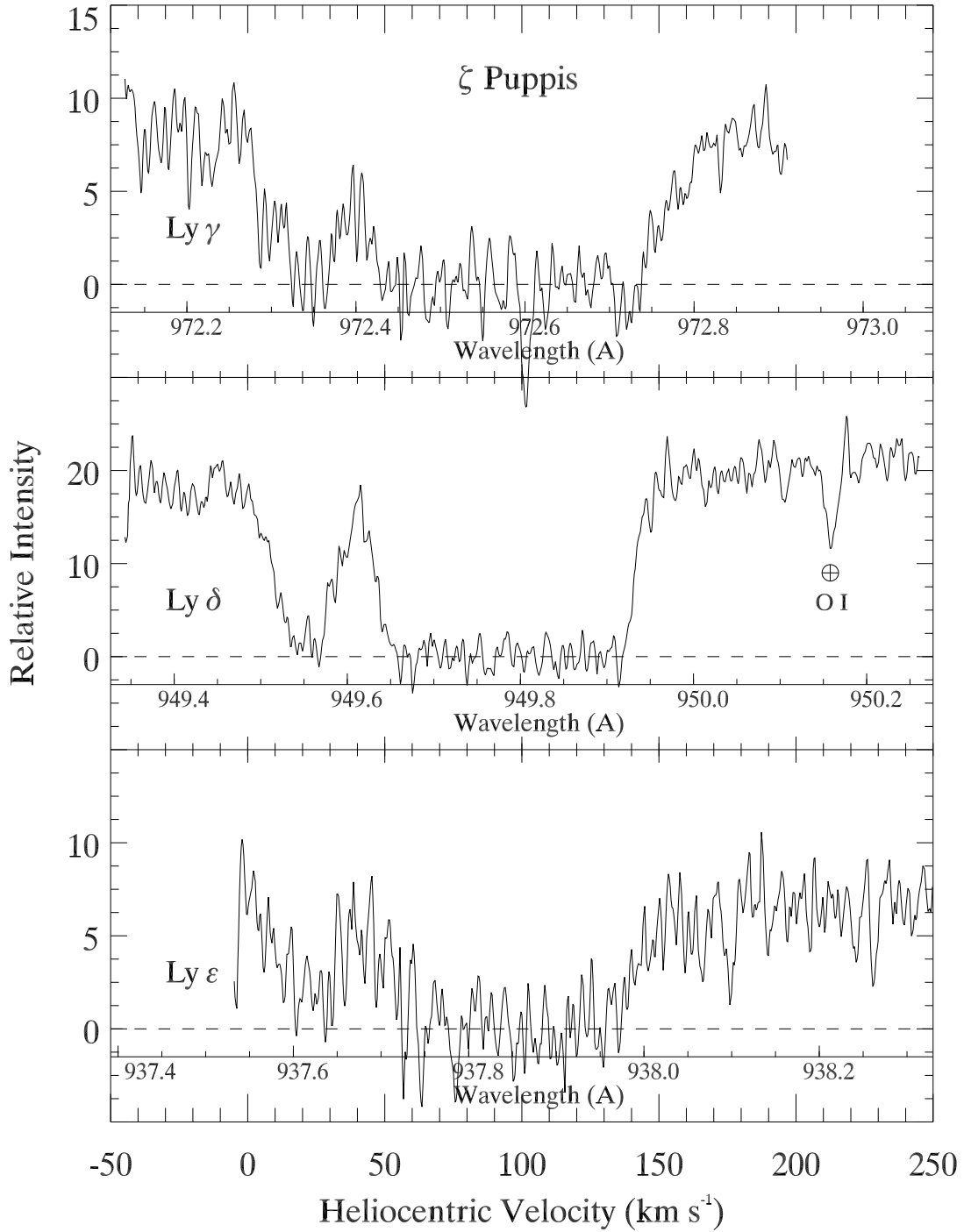


Fig. 2.— Line profiles of Ly γ , Ly δ , and Ly ϵ from IMAPS spectra for ζ Pup. The zero-point of the velocity scale is computed with respect to the laboratory wavelengths of the D I lines.

3.2. Velocity Profile Templates

In Paper I we discussed the benefits of obtaining a velocity profile based on high quality data for N I and O I, two species that are not significantly depleted in the ISM and which have very similar ionization balances to those of D I and H I (Ferlet 1981; York et al. 1983). This profile information is helpful in constraining the variety of possible interpretations that would produce acceptable fits with the D profiles. For N I, we used IMAPS spectra of the 10 lines in the multiplets at 952.4, 953.8, 954.1 and 1134.7 Å⁷. For all of the N I lines except those in the 952.4 Å multiplet, the background level was easily defined because the stronger lines were saturated. Of course, these lines were useful only for defining the behavior of the gas at velocities somewhat removed from the line core. Since the lines in the multiplet at 952.4 Å were not saturated, we had to determine the background level by a different method. For both γ^2 Vel and ζ Pup, there are U1 scans of this weak multiplet available in the archive of spectra recorded by the *Copernicus* satellite (Rogerson et al. 1973). After comparing our IMAPS spectrum degraded to the resolution of *Copernicus* with the actual *Copernicus* scans, we determined the adjustments to the background levels that were needed for the IMAPS spectra of this N I multiplet. The backgrounds caused by grating scatter in the *Copernicus* spectra were taken from the observed count rates in the bottoms of the hydrogen Ly γ and Ly δ lines, and these levels were subtracted off before the comparison was made.

As was done for our analysis in Paper I, we adopted a method developed by Jenkins & Peimbert (1997) to create a composite profile for the column density of N I as a function of velocity from the 10 lines in the four multiplets, with the weak lines in each case defining the main part of the profile and the strong lines outlining the exact shape of the profile’s wings, well away from the saturated part of the line. For places where there was overlap in the useful portions of the lines, there was satisfactory agreement. The f -values of Goldbach et al. (1992) were adopted for our analysis.

Figure 3 shows the $N_a(v)$ profiles derived for N I toward γ^2 Vel and ζ Pup. In Paper I we showed that the profiles are unlikely to be contaminated by additional contributions from telluric absorption. $N(\text{N I})$ is $\sim 1\%$ of $N(\text{O I})$ in the Earth’s atmosphere at the altitude of IMAPS (~ 305 km) during the *ORFEUS-SPAS II* mission. Even for our strongest N I transition used to derive the far wings of $N_a(v)$ for N I ($\lambda 1134.98$), the telluric absorption should be only one third as strong as the O I* $\lambda 950.112$ feature present in Figures 1 and 2, and at a heliocentric velocity of $+12.6 \text{ km s}^{-1}$ it would be buried in the saturated portion of the profile. Consequently, telluric N I has a negligible effect on the interstellar N I profiles.

O I is the best tracer of H I in the ISM since the ionization potential of O I (13.56 eV) is nearly identical to that of H I. The ionization potential of N I (14.53 eV) is only slightly greater than that of H I. Furthermore, both O and N are coupled to H by resonant charge exchange

⁷One of the lines in the 1134.7 Å multiplet, the line at 1134.165 Å, had to be omitted from consideration for ζ Pup because it was too close to the edge of the image format.

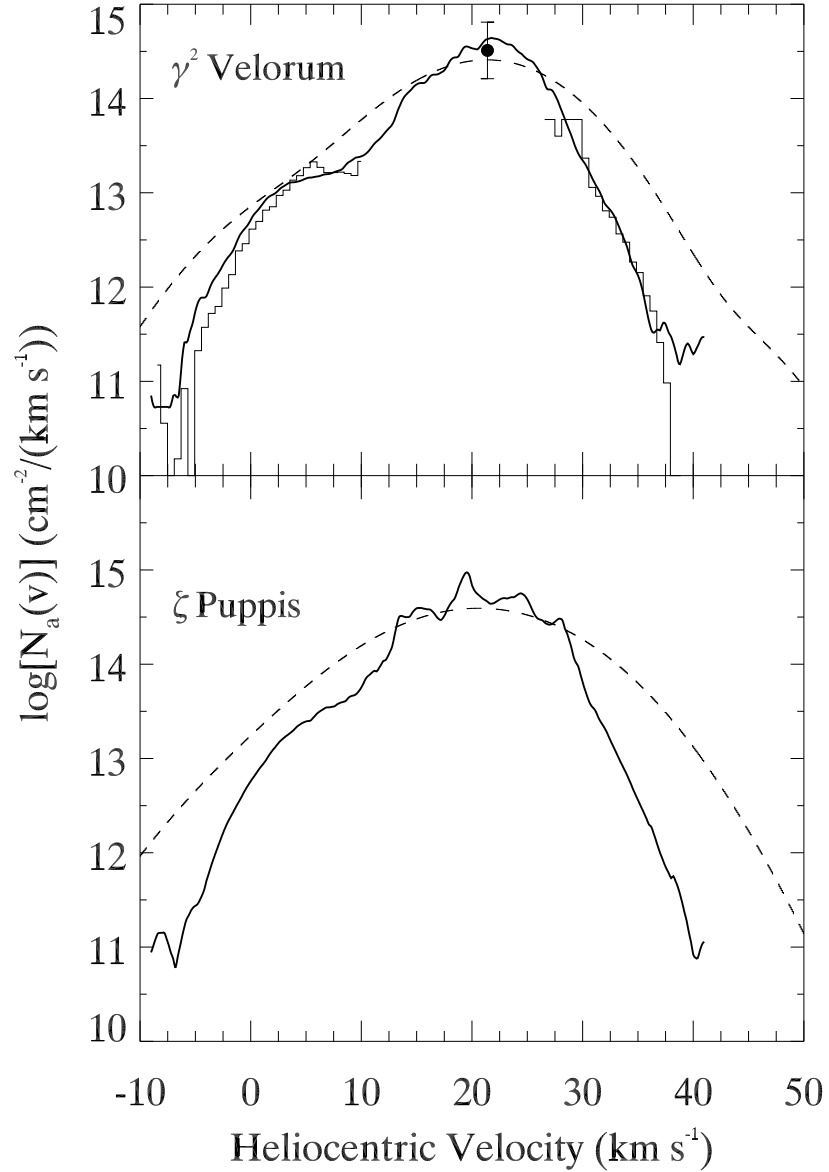


Fig. 3.— Profiles for $N_a(v)$ (thick solid lines) for N I toward γ^2 Vel and ζ Pup derived from IMAPS spectra. For γ^2 Vel, $N_a(v)$ for the wings of O I $\lambda 1039.23$, adjusted for the difference in cosmic abundance between O and N (-0.90 dex), is shown by the thin histogram line. The single data point and error bar correspond to $N(\text{O I})$ from Fitzpatrick & Spitzer (1994) for O I $\lambda 1355.6$ (see text for details). The dashed lines show the expected shapes of the D I profiles for a thermal broadening for $T = 6070$ K (γ^2 Vel) and $T = 9550$ K (ζ Pup) of the respective N I profile favored by our most likely solutions in Tables 2 and 3.

reactions. As discussed by Sofia & Jenkins (1998) and Jenkins et al. (2000), N I closely follows O I and H I unless $n_e \gg n_{\text{HI}}$.

In the IMAPS wavelength band there is no suitable set of O I transitions to completely define a velocity profile template. The available O I lines are highly saturated or are not detectable, either because they are buried in the core of a Lyman series line or because they are too weak. In Paper I we made use of an archival *HST* spectrum of the very weak intersystem transition of O I at 1355.6 Å for δ Ori A. There is no such spectrum available for ζ Pup, and the measurement of this line in the spectrum of γ^2 Vel taken by Fitzpatrick & Spitzer (1994) is too noisy to adequately define the shape of the O I profile. Therefore, we were forced to use the next best option, N I, to define the velocity profile template.

Although we do not have a complete $N_a(v)$ profile for O I, we tested the assumption that N I traces H I by comparing selected portions of the O I $N_a(v)$ profile derived from available line profiles in γ^2 Vel. First, we computed $N_a(v)$ from the wings of O I $\lambda 1039.230$. Second, we used the GHRS spectrum of O I $\lambda 1355.6$ (Fitzpatrick & Spitzer 1994) to define $N_a(v)$ in the core of the line. The computed $N_a(v)$ was scaled by the difference in the N and O solar abundances (-0.90 dex, Anders & Grevesse 1989). The results, shown in Fig 3, demonstrate that the wings and core of $N_a(v)$ for N I and O I are in excellent agreement. Consequently, we have high confidence that the $N_a(v)$ profile for N I provides an accurate model for the velocity distribution of H I.

3.3. γ^2 Velorum

The continuum near the Ly δ line shown in Figure 1 was determined in the velocity range $(-40, -10)$ km s $^{-1}$ on the blue side of the D I line and $(+170, +205)$ km s $^{-1}$ on the red side. For Ly ϵ , the continuum limits were $(-14, +8)$ km s $^{-1}$ and $(+170, +210)$ km s $^{-1}$. The background level was determined from the core of the two H I lines in the velocity range $(+60, +140)$ km s $^{-1}$. The D I profiles were fit in the velocity range $(-10, +39)$ km s $^{-1}$ for Ly δ and $(+8, +39)$ km s $^{-1}$ for Ly ϵ . With a spacing of independent velocity samples of 1.25 km s $^{-1}$, this resulted in 276 degrees of freedom in the χ^2 analysis to fit the 10 free parameters described in §3.1.

By adjusting our estimate for the noise, which was only known to limited accuracy beforehand, we achieved a minimum value for χ^2 equal to 247.0 at a column density of 1.12×10^{15} cm $^{-2}$. For 276 degrees of freedom, there was a 90% chance that we would have found this value of χ^2 or greater. With this 90% confidence level, we arrived at a conservatively high estimate for the noise. It then followed that this noise level, which is perhaps higher than the real noise, gave a conservatively large confidence interval for $N(\text{D I})$, as determined by how rapidly the values of χ^2 deviated from the minimum value. With the noise level having been set in the manner just described, we explored for 90% and 99% confidence limits for $N(\text{D I})$ (i.e., 1.65σ and 2.58σ deviations), which correspond to $\chi^2(\text{min})+4.6$ and $\chi^2(\text{min})+9.2$, respectively. Table 2 lists $N(\text{D I})$ and T for the best value and these limits. The $\pm 90\%$ confidence limits on the model D I profiles

(*cross-hatched regions*) for Ly δ and Ly ϵ are compared with the observed deuterium profiles in Figure 4.

In Figure 4 we also show with a *dashed line* the expected shape and depth of the D I profile for $N(\text{D I}) = 7.7 \times 10^{14} \text{ cm}^{-2}$. This corresponds to a D/H ratio of 1.5×10^{-5} , assuming the H I column density derived below in §4. For this case, $\chi^2 - \chi^2(\text{min}) = 52.4$, which is clearly an unacceptable fit. The *dot-dashed line* in Figure 4 corresponds to the D I profile for $N(\text{D I}) = 3.8 \times 10^{14} \text{ cm}^{-2}$, the D I column density necessary to achieve D/H = 0.74×10^{-5} , the value found toward δ Ori A in Paper I. A similar demonstration for the measurement of $N(\text{H I})$ is given in §5.

3.4. ζ Puppis

The measurement of $N(\text{D I})$ toward ζ Pup used the same methodology described in the previous section with the following modifications. In addition to Ly δ and Ly ϵ we were able to include the D I profile of Ly γ in the χ^2 analysis. The blue and red regions for the linear continuum fits were $(-40, -10) \text{ km s}^{-1}$ and $(+170, +190) \text{ km s}^{-1}$ for Ly γ , $(-39, -10) \text{ km s}^{-1}$ and $(+157, +190) \text{ km s}^{-1}$ for Ly δ , and $(-4, +3) \text{ km s}^{-1}$ and $(+180, +220) \text{ km s}^{-1}$ for Ly ϵ . The background levels were determined from the saturated cores of the H I lines over these velocity limits: $(+55, +130)$ for Ly γ and Ly δ , $(+65, +115)$ for Ly ϵ . The model D I profiles were fit over the range $(-5, +40) \text{ km s}^{-1}$ for Ly γ , $(0, +40) \text{ km s}^{-1}$ for Ly δ , and $(+3, +37) \text{ km s}^{-1}$ for Ly ϵ . This resulted in 426 degrees of freedom to simultaneously fit the 13 free parameters described in §3.1. The minimum χ^2 is 388.5 and corresponds to the most probable value of $N(\text{D I})$ for ζ Pup, namely $1.30 \times 10^{15} \text{ cm}^{-2}$. The results of the χ^2 analysis are summarized in Table 3, including the 90% and 99% confidence limits. The same conservative treatment of the noise described for γ^2 Vel was followed for ζ Pup. Figure 5 shows the observed D I Lyman line profiles and the range in the best fit model profiles and continua fits allowed by the 90% confidence limits.

Table 2. Limits for $N(\text{D I})$ Toward γ^2 Vel

Significance	$N(\text{D I})$ (10^{15} cm^{-2})	T (K)	χ^2
Minimum $N(\text{D I})$ at the 99% confidence limit	0.96	6630	255.6
Minimum $N(\text{D I})$ at the 90% confidence limit	1.00	6530	251.6
Best $N(\text{D I})$	1.12	6070	247.0
Maximum $N(\text{D I})$ at the 90% confidence limit	1.27	5280	251.7
Maximum $N(\text{D I})$ at the 99% confidence limit	1.34	4870	256.1

Table 3. Limits for $N(\text{D I})$ Toward ζ Pup

Significance	$N(\text{D I})$ (10^{15} cm^{-2})	T (K)	χ^2
Minimum $N(\text{D I})$ at the 99% confidence limit	1.07	10600	397.7
Minimum $N(\text{D I})$ at the 90% confidence limit	1.13	10400	393.1
Best $N(\text{D I})$	1.30	9550	388.5
Maximum $N(\text{D I})$ at the 90% confidence limit	1.49	8500	393.1
Maximum $N(\text{D I})$ at the 99% confidence limit	1.58	7900	397.7

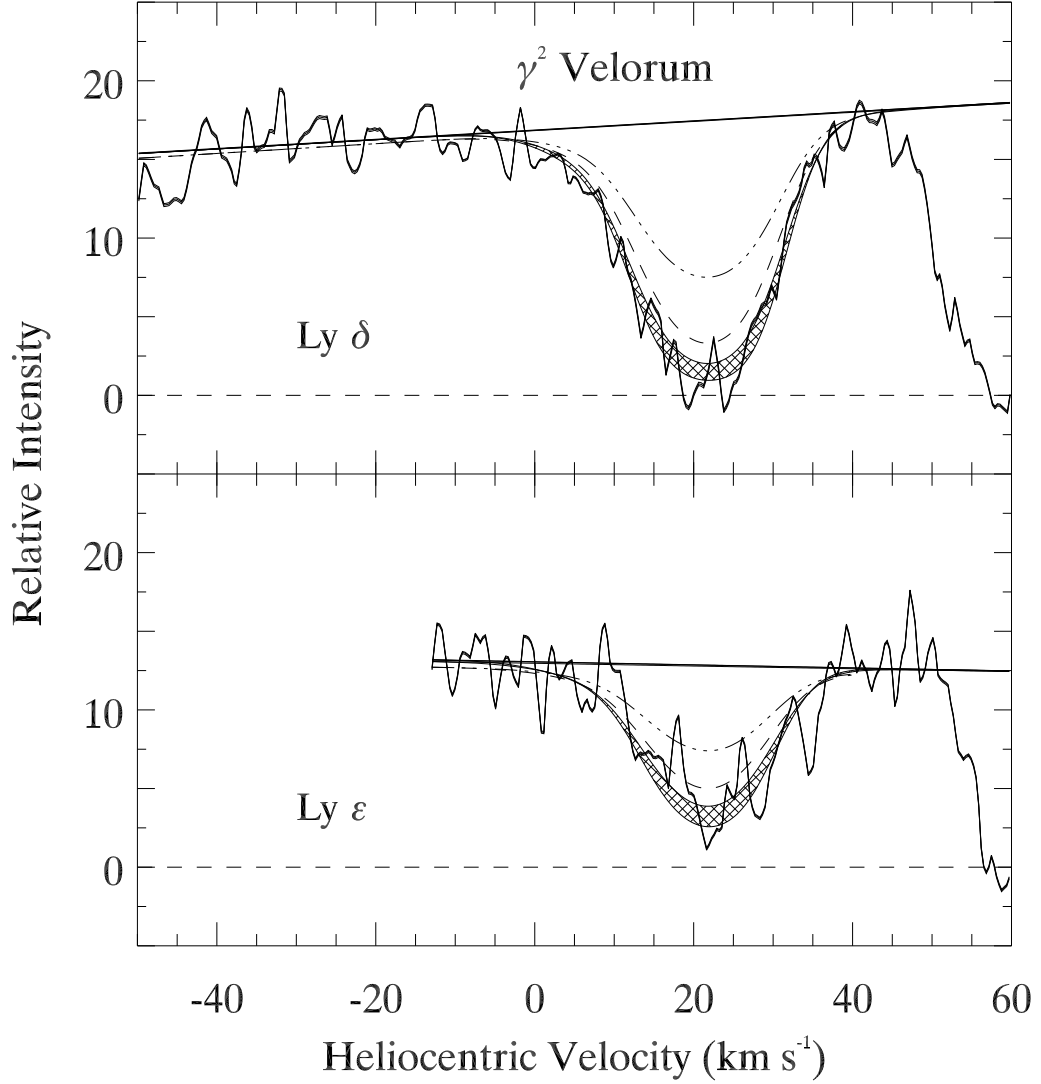


Fig. 4.— Observed and model line profiles of D I Ly δ and Ly ϵ for γ^2 Vel showing the region bounded by the 90% confidence limits on $N(\text{D I})$ (cross-hatched region), derived from both lines collectively. Assuming the value of $N(\text{H I})$ derived for γ^2 Vel in §4, the dashed line illustrates the D I line shapes necessary to achieve $\text{D}/\text{H} = 1.5 \times 10^{-5}$ and the dot-dashed line corresponds to the D I profiles necessary to obtain $\text{D}/\text{H} = 0.74 \times 10^{-5}$ (δ Ori A, Paper I).

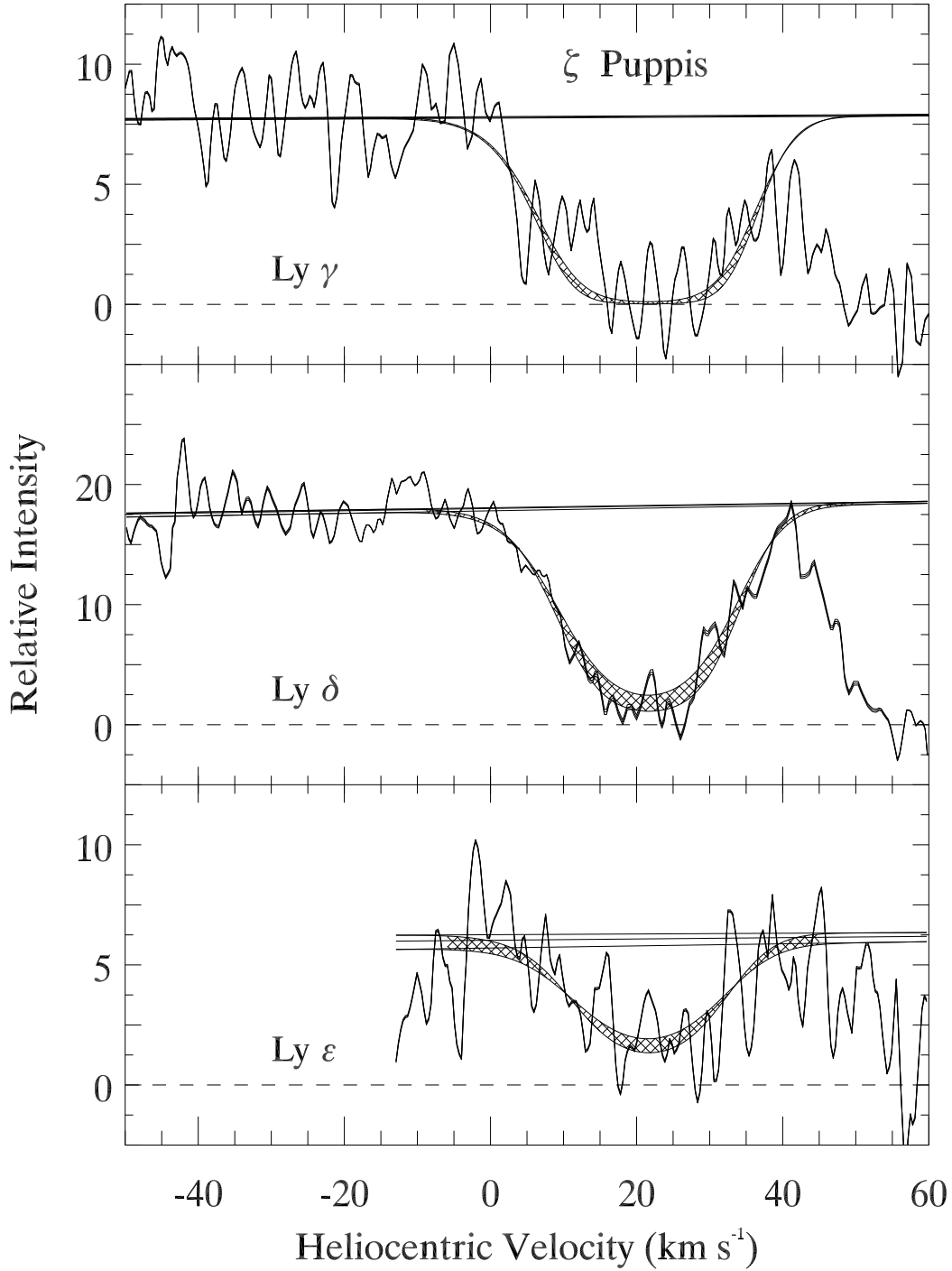


Fig. 5.— Observed and model line profiles of D I Ly γ , Ly δ , and Ly ϵ for ζ Pup showing the region bounded by the 90% confidence limits on $N(\text{D I})$ (cross-hatched region), derived from all three lines collectively. Note that the preferred continuum levels near Ly ϵ change for different values of $N(\text{D I})$.

4. COLUMN DENSITY OF ATOMIC HYDROGEN

4.1. Analysis Methodology

The primary objective of this IMAPS program is to determine D/H ratios of sufficient accuracy to test for spatial inhomogeneities. To achieve this goal, we must strive for a precision in $N(\text{H I})$ that is as good as (or preferably better than) that of the deuterium measurement. We must also understand the magnitude and nature of the uncertainties in $N(\text{H I})$ and $N(\text{D I})$ so that we can realistically assess the uncertainty in D/H for comparison to other measurements in the ISM. For these reasons, we decided to conduct our own investigation of the H I column densities toward γ^2 Vel and ζ Pup, even though a number of measurements of $N(\text{H I})$ toward these stars are already available in the literature (e.g. Jenkins 1971; York & Rogerson 1976; Vidal-Madjar et al. 1977; Bohlin, Savage, & Drake 1978; Shull & Van Steenberg 1985; Diplas & Savage 1994).

We described our method for determining $N(\text{H I})$ in Paper I; here we provide a summary. In §4.2 and §4.3 we discuss details particular to the ζ Pup and γ^2 Vel sight lines and present the results. We used the Ly α line to determine the total $N(\text{H I})$.⁸ Since H I Ly γ and Ly δ are on the flat part of the curve of growth, high velocity gas could influence their profiles. Ly α is immune from this potential problem. Due to the great breadth of the Lorentzian wings ($\pm 1000 \text{ km s}^{-1}$ – see the velocity scale in Figure 9), Ly α absorption due to any high velocity interstellar gas ($\pm 100 \text{ km s}^{-1}$) that may be present is confined to the saturated core of the profile. In principle, some high velocity H I, which is too widely dispersed in velocity to show up in the D I profiles, could contribute to the Ly α damping wings. However, this gas is not detected in the strong lines N I $\lambda 1134.98$ and O I $\lambda 1039.23$ observed with IMAPS. It is clear that such high velocity gas, if present, would have a low column density and a negligible effect on the Ly α damping wings. Since the Ly α line is not covered by IMAPS, was not observed by the *HST* spectrographs, and the available *Copernicus* Ly α scans suffer from several problems (see Paper I), we analyzed high dispersion *IUE* observations of Ly α to determine $N(\text{H I})$. Furthermore, these stars were observed many times with *IUE* over the course of many years, and this offers an opportunity to evaluate potential sources of systematic error. For example, γ^2 Vel is a spectroscopic binary, and the large *IUE* database allowed a search for systematic changes in the derived $N(\text{H I})$ as a function of orbital phase.

After screening and retrieving the *IUE* data⁹ of interest and correcting for interorder scattered light (see Paper I), we used an approach first used by Jenkins (1971) to constrain the H I column

⁸The *Copernicus* studies of D/H on the γ^2 Vel and ζ Pup sight lines used the much weaker damping wings of Ly β or Ly γ to determine $N(\text{H I})$.

⁹We used the standard IUESIPS calibration of the *IUE* high dispersion spectra instead of the NEWSIPS calibration to avoid potential problems with background corrections and zero-level determination near Ly α found in some *IUE* SWP high dispersion spectra processed with NEWSIPS (see Massa et al. 1998), which could adversely affect our measurements.

density, i.e., we determined the $N(\text{H I})$ which provides the best fit to the $\text{Ly}\alpha$ profile with the optical depth τ at a given wavelength λ calculated from the expression

$$\tau(\lambda) = N(\text{H I})\sigma(\lambda) = 4.26 \times 10^{-20} N(\text{H I})(\lambda - \lambda_0)^{-2} \quad (1)$$

where λ_0 is the $\text{Ly}\alpha$ line center at the velocity centroid of the hydrogen (note that the useful portion of the $\text{Ly}\alpha$ profile is entirely due to the Lorentzian wings and the effects of instrumental and Doppler broadening can be neglected). As was done for D I, we also determined the important free parameters which can be adjusted to fit the H I $\text{Ly}\alpha$ absorption profile, then we found the set of parameters that minimized χ^2 using Powell’s method. We set confidence limits on the H I column as described in §3.1 with only one parameter of interest, $N(\text{H I})$. The other (uninteresting) free parameters we selected for fitting the H I profile were three coefficients which specify a second-order polynomial fit to the continuum, and an additive correction to the flux zero point. The continuum was fit to the spectrum in several windows covering the range 1185 Å to 1276 Å. Despite our use of the Bianchi & Bohlin (1984) correction for interorder scattered light, in many cases inspection of the flat-bottomed, saturated portion of the $\text{Ly}\alpha$ profile showed that the zero intensity level was not quite correct. A zero point shift in the flux scale, one of the terms for evaluating χ^2 , was determined from a region within the saturated core. For both stars, the zero point of the $\text{Ly}\alpha$ wavelength scale was set by placing the N I $\lambda 1200$ multiplet in agreement with the IMAPS N I profiles. The $\text{Ly}\alpha$ profile was then fit only to the red wing because of the presence of strong stellar features superposed on the blue wing. However, the uncontaminated portion of the blue wing of $\text{Ly}\alpha$ was checked for consistency with the fit to the red wing and found to be in good agreement.

4.2. ζ Puppis

In Paper I, considerable attention was paid to the spectroscopic binary nature of δ Ori A and whether or not this could cause systematic errors in $N(\text{H I})$. A similar analysis of γ^2 Vel is presented in §4.3. The determination of $N(\text{H I})$ toward ζ Pup was less complex than the other stars observed by IMAPS to study D/H. As far as is known, ζ Pup is not a spectroscopic binary star. It is an O4 supergiant, so the stellar H I $\text{Ly}\alpha$ absorption line makes a negligible contribution to the H I absorption profile. The star is possibly a non-radial pulsator with very weakly variable stellar absorption lines with a period of 8.5 hr (Reid & Howarth 1996), and the variability of the stellar wind P-Cygni profiles is well known and studied (e.g., Prinja et al. 1992; Howarth, Prinja, & Massa 1995) and shows significant power at 19.2 hr and 5.2 day periods. Both of these sources of spectral variations are expected to have little impact on the interstellar H I column density derived from $\text{Ly}\alpha$, but this can be checked given the large number of observations and good temporal sampling.

There are more than 200 high-dispersion observations of ζ Pup in the *IUE* archive, primarily because the star was selected for intensive *IUE* observing programs to study stellar wind variability

in massive stars. We concentrated on the spectra obtained in three specific multi-day observing runs in 1986, 1989, and 1995. In 1995 ζ Pup was observed continuously for 16 days (dubbed the "MEGA" campaign, Massa et al. 1995). We omitted three observations from these observing sessions because the archival data were corrupted or unavailable. This left 189 observations for measurement of $N(\text{H I})$. All of the observations were obtained with the *IUE* large aperture and the signal-to-noise ratios are comparable; the ζ Pup data set is more uniform than the *IUE* Ly α data used for measuring $N(\text{H I})$ toward δ Ori A and γ^2 Vel.

The $N(\text{H I})$ values derived from each individual observation are plotted in Figure 6, along with the 1σ uncertainties, versus the observation date. Table 4 summarizes the mean H I column density $\langle N(\text{H I}) \rangle$ and the root mean square (rms) dispersion σ obtained from the 1986, 1989, and 1995 data sets analyzed separately, and $\langle N(\text{H I}) \rangle$ for each data set is indicated with a heavy dashed line in Figure 6. We also list in Table 4 the formal error in the mean $\epsilon = \sigma/\sqrt{N}$ (here N is the number of measurements) and the reduced χ^2 for the three data sets.

In Paper I we discussed the potential sources of systematic error in the derivation of $N(\text{H I})$ from *IUE* spectra, and we suggested that the real uncertainty in the mean is likely to be greater than the formal estimate. The very large Ly α data set for ζ Pup shown in Figure 6 appears to confirm that this is indeed the case for this star. From this figure one can see that the column densities derived from the 1995 data are systematically lower than the column densities derived from the 1989 observing run. The mean of the 1995 data set is lower than the mean of the 1989 data by $0.54 \times 10^{19} \text{ cm}^{-2}$ (0.0256 dex), and this difference is substantially greater than the formal error estimates (ϵ).

This systematic error could be the result of secular changes in the stellar mass loss or circumstellar environment, a previously unrecognized stellar variability with a long period, or instrumental effects. Or perhaps some aspect of the interstellar sight line changed during this period. Since the IMAPS observations for $N(\text{D I})$ were made almost two years after the MEGA campaign, it is possible that a similar systematic error is present in any *IUE* estimate of $N(\text{H I})$ that we choose for comparison with the IMAPS $N(\text{D I})$. The exact magnitude of this systematic uncertainty is difficult to estimate, but we find that $N(\text{H I})$ obtained from additional large aperture spectra of ζ Pup taken at other epochs are in good agreement with the estimates in Table 4. This indicates that the systematic error is not much larger than 0.0256 dex. For example, large aperture observations taken in 1988 May, 1989 December, and 1991 March, combined with the three $\langle N(\text{H I}) \rangle$ values for the three data sets in Table 4, yield a mean $N(\text{H I}) = 9.34 \pm 0.67 \times 10^{19} \text{ cm}^{-2}$. We conclude that 0.0256 dex is a conservative estimate of the 1σ uncertainty in $N(\text{H I})$. We therefore adopt the unweighted mean of the three $\langle N(\text{H I}) \rangle$ values in Table 4 as the best estimate of $N(\text{H I})$ toward ζ Pup and 0.0256 dex as its 1σ uncertainty: $N(\text{H I}) = 9.18 \pm 0.54 \times 10^{19} \text{ cm}^{-2}$. We elected to use a mean of the $\langle N(\text{H I}) \rangle$ values in Table 4 instead of a straight mean of all of the individual measurements shown in Fig. 6 because the latter would give excessive weight to the 1995 data set due to the much larger number of measurements obtained during that observing campaign.

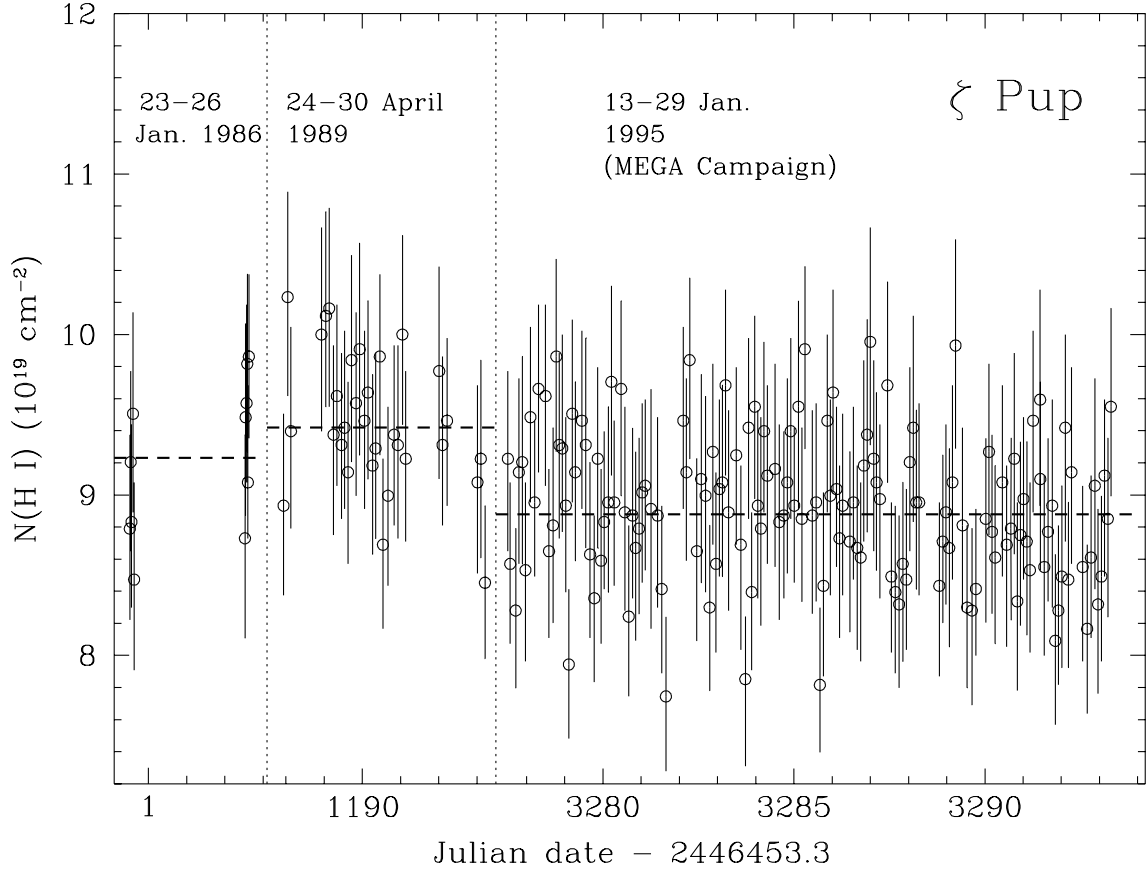


Fig. 6.— H I column densities toward ζ Pup derived from the 189 high-dispersion *IUE* observations obtained in 1986, 1989, and 1995, plotted versus the observation date. Each measurement is shown with $\pm 1\sigma$ error bars. All observations were obtained with the large aperture and have comparable signal-to-noise ratios. Each data set is separated by a vertical dotted line (i.e., there is a break in the x-axis at each vertical dotted line), and the mean H I column densities derived from the three data sets are indicated with heavy dashed lines. There appears to be a systematic difference between the column densities derived from the 1995 data and the earlier observations.

Table 4. Interstellar $N(\text{H I})$ Toward ζ Pup

Data Set ^a	No. Spectra	$\langle N(\text{H I}) \rangle$ (cm^{-2})	σ^{b} (cm^{-2})	ϵ^{c} (cm^{-2})	χ_{ν}^2 ^d
1986	11	9.23×10^{19}	0.47×10^{19}	0.14×10^{19}	0.69
1989	31	9.42×10^{19}	0.43×10^{19}	0.08×10^{19}	0.56
1995 ^e	147	8.88×10^{19}	0.46×10^{19}	0.04×10^{19}	0.69
Adopted value ^f	189	9.18×10^{19}

^aAll $N(\text{H I})$ measurements were derived from *IUE* high dispersion spectra using the large aperture. We have used only the observations obtained during three observing runs in 1986, 1989, and 1995. This table shows the mean H I column density, $\langle N(\text{H I}) \rangle$, derived from the 1986 data only, the 1989 data only, and the 1995 data only.

^b σ = rms dispersion (both σ and $\langle N(\text{H I}) \rangle$ were weighted inversely by the variances of the individual $N(\text{H I})$ measurements).

^c ϵ = error in the mean = $\sigma / (\text{No. measurements})^{0.5}$.

^dReduced χ_{ν}^2 = $\chi^2 / (\text{degrees of freedom})$, where $\chi^2 = \sum_i \{ [N_i(\text{H I}) - \langle N(\text{H I}) \rangle] / \sigma [N(\text{H I})]_i \}^2$.

^eThe *IUE* MEGA campaign (Massa et al. 1995).

^fFinal adopted value of $N(\text{H I})$ is the average of $\langle N(\text{H I}) \rangle$ for the three data sets. See text for details.

4.3. γ^2 Velorum

As noted in §1, γ^2 Vel is a complex stellar system with a strongly variable UV stellar spectrum. Figure 7 shows two examples of the high-dispersion *IUE* spectra of γ^2 Vel that we have used to derive $N(\text{H I})$. These examples were selected to illustrate the variability of the P-Cygni emission lines in the vicinity of $\text{Ly}\alpha$, which are weakest at orbital phase ~ 0.5 . Figure 7 also shows the complex and variable stellar absorption superposed on much of the blue wing of the interstellar $\text{Ly}\alpha$ profile. This variability was a source of concern for this paper. Can we derive reliable H I column densities despite the complex spectral changes occurring in this star? Due to the stellar absorption, the blue wing of $\text{Ly}\alpha$ was not useful for constraining $N(\text{H I})$. Fortunately, the red wing of $\text{Ly}\alpha$ was clean and stable as a function of orbital phase. This can be seen by comparing panel (a) to panel (b) in Figure 7. In this paper, we used only the red wing for fitting the $\text{Ly}\alpha$ profile, and the resultant fits generally look quite good (see Figures 7 and 9).

We examined $N(\text{H I})$ as a function of orbital phase of the spectroscopic binary to check for systematic errors in the derived interstellar H I column density due to the complicated variability of the stellar spectrum. There are considerable discrepancies in the orbital elements published by various groups (Stickland & Lloyd 1990; Schmutz et al. 1997, and references therein). We adopt the orbital elements derived by Schmutz et al. (1997) who find a period of $78^{\text{d}}53 \pm 0^{\text{d}}01$ d with velocity semiamplitudes of $K_{\text{WR}} = 122 \pm 2$ km s $^{-1}$ and $K_{\text{O}} = 38.4 \pm 2$ km s $^{-1}$. In addition to the usual intrinsic variability of WR stars, it is believed that the γ^2 Vel spectrum may also change as a result of periodic absorption of the O star component by the WR wind (Stickland & Lloyd 1990).

After screening the *IUE* high-dispersion observations of γ^2 Vel, we were left with 42 spectra, 34 small aperture observations obtained early in the *IUE* mission and 8 later observations obtained with the large aperture. In Figure 8 we plot the H I column densities derived from all of the observations as a function of the phase of the spectroscopic binary, and Table 5 summarizes the $\langle N(\text{H I}) \rangle$, σ , and ϵ derived from the large aperture data only, the small aperture data only, and all of the data combined. While one might argue that a trend is apparent in Figure 8 with a minimum in the derived $N(\text{H I})$ values at orbital phase ~ 0.5 , this is a marginal result at best, and we do not believe that it should be taken too seriously. On the contrary, the generally good agreement of the H I column densities at various phases despite the dramatic changes in the stellar spectrum (see Figure 7) is encouraging, and we conclude from Figure 8 that the *IUE* data provide a good determination of $\langle N(\text{H I}) \rangle$. Since the small and large aperture measurements are in good agreement, we adopted the results from the combined data set. Systematic errors probably cause the true uncertainty in $\langle N(\text{H I}) \rangle$ to exceed the formal error estimate provided in Table 5. Drawing from our experience with the more extensive data set for ζ Pup, we conservatively adopt 0.0256 dex as the 1σ uncertainty in $N(\text{H I})$ toward γ^2 Vel as well: $N(\text{H I}) = 5.13 \pm 0.30 \times 10^{19}$ cm $^{-2}$.

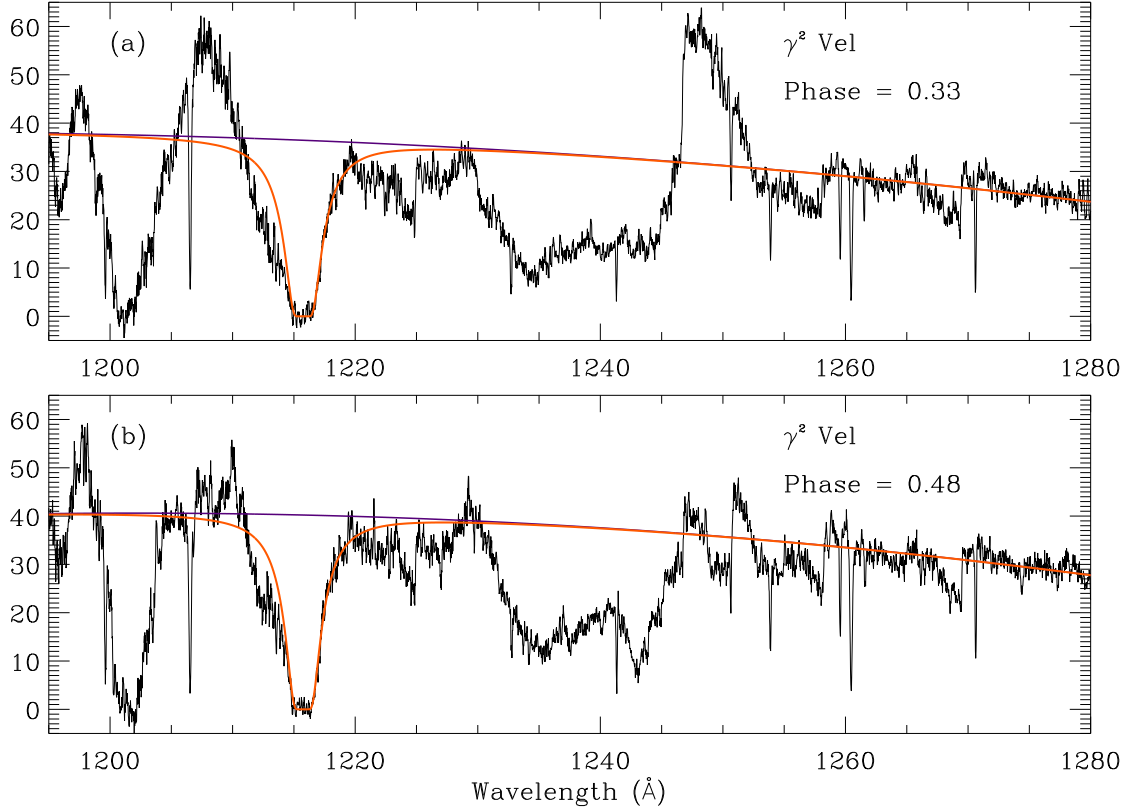


Fig. 7.— Samples of the *IUE* observations of γ^2 Vel used to derive the interstellar $N(\text{H I})$: (a) SWP6175, spectroscopic binary phase = 0.33, and (b) SWP4719, phase = 0.48 (phases were calculated using the period and T_0 from Schmutz et al. 1997). These spectra have been smoothed with a 5-pixel boxcar for display purposes only; the unsmoothed data were used to constrain $N(\text{H I})$ as described in the text. The best-fitting H I profiles (dotted lines) and continua (dashed lines) are overplotted on the data. Note the dramatic variability of the P-Cygni profiles. Note also the presence of complicated absorption structure which makes the blue wing of the Ly α profile difficult to use for constraining $N(\text{H I})$. Both of these observations were obtained with the small *IUE* aperture.

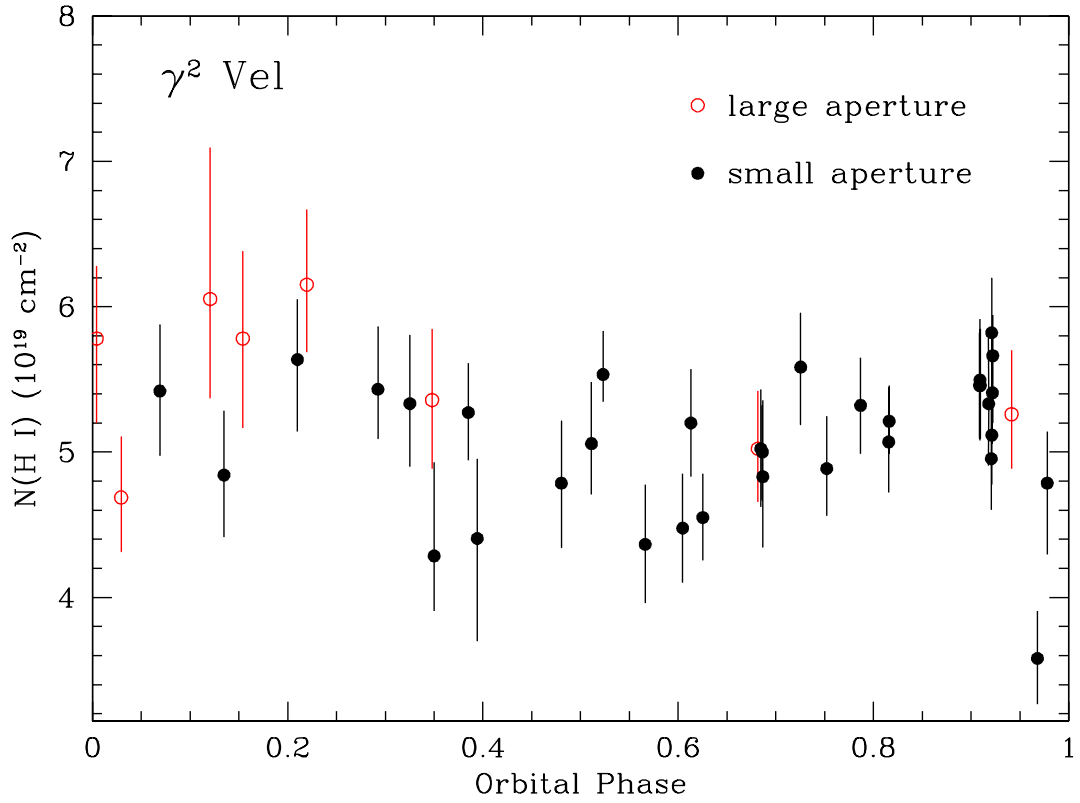


Fig. 8.— Interstellar H I column densities derived from the 42 *IUE* observations of γ^2 Vel, plotted versus phase of the spectroscopic binary. Each column density is plotted with $\pm 1\sigma$ error bars. Data obtained with the large aperture are indicated with open circles while small aperture results are shown with filled circles.

Table 5. Interstellar $N(\text{H I})$ Toward γ^2 Vel

Data Set ^a	No. Spectra	$\langle N(\text{H I}) \rangle$ (cm^{-2})	σ^{b} (cm^{-2})	ϵ^{c} (cm^{-2})	χ_{ν}^2 ^d
Lg. Aperture	8	5.35×10^{19}	0.51×10^{19}	0.18×10^{19}	1.15
Sm. Aperture	34	5.10×10^{19}	0.48×10^{19}	0.08×10^{19}	1.71
All Data	42	5.13×10^{19}	0.49×10^{19}	0.08×10^{19}	1.62

^aAll $N(\text{H I})$ measurements were derived from *IUE* high dispersion spectra. This table shows the mean H I column density, $\langle N(\text{H I}) \rangle$, derived from the large *IUE* aperture data only, the small aperture data only, and all of the data combined.

^b σ = rms dispersion (both σ and $\langle N(\text{H I}) \rangle$ were weighted inversely by the variances of the individual $N(\text{H I})$ measurements).

^c ϵ = error in the mean = $\sigma/(\text{No. measurements})^{0.5}$.

^dReduced $\chi_{\nu}^2 = \chi^2/(\text{degrees of freedom})$, where $\chi^2 = \sum_i \{[N_i(\text{H I}) - \langle N(\text{H I}) \rangle] / \sigma [N(\text{H I})]_i\}^2$.

5. DEUTERIUM AND NITROGEN ABUNDANCE RATIOS

5.1. D/H

Combining the results for D I and H I column densities derived in the previous sections, we determined the atomic D/H abundance ratio for γ^2 Vel and ζ Pup. Toward γ^2 Vel we found that $D/H = 2.18_{-0.31}^{+0.36} \times 10^{-5}$ (the errors are 90% confidence limits). This result is a large departure from the value of D/H usually attributed as “typical” in the ISM of the Galaxy ($\sim 1.5 \times 10^{-5}$). A large value for the average D/H ratio implies that even larger values could exist in individual components if other components have lower D/H values closer to the LISM ratio. Although the previous D/H measurement for γ^2 Vel ($= 2.0_{-0.7}^{+1.1} \times 10^{-5}$, York & Rogerson 1976) appears to be in close agreement with the IMAPS result, we consider this to be coincidental in view of the magnitude of the uncertainties in the *Copernicus* measurement.

For ζ Pup we find $N(\text{D I}) = 1.30_{-0.17}^{+0.19} \times 10^{15} \text{ cm}^{-2}$, a value slightly below the lower limit derived from *Copernicus* spectra by Vidal-Madjar et al. (1977). They found that a large range in $N(\text{D I})$ ($1.5 - 20. \times 10^{15} \text{ cm}^{-2}$) was possible for this sight line due to its complexity and a lack of adequate constraints. Since the value of $N(\text{H I})$ derived by Vidal-Madjar et al. (1977) for ζ Pup is consistent with ours, their large range in D/H must be a result of the $N(\text{D I})$ uncertainty. Much more is known now about the complexity of this sightline than at the time of the *Copernicus* study (e.g. Welty, Morton & Hobbs 1996). More importantly, the IMAPS spectra have sufficient spectral resolution that the structure of the ζ Pup sightline in neutral hydrogen can be defined by the $N_a(v)$ profile for N I and used to constrain the determination of $N(\text{D I})$. Thus with higher spectral resolution and better knowledge of the velocity structure along the sightline, a more accurate value of $N(\text{D I})$ and D/H is derived. We find $D/H = 1.42_{-0.23}^{+0.25} \times 10^{-5}$. The $N(\text{D I})$, $N(\text{H I})$, and D/H results for the three stars studied by IMAPS are summarized in Table 6, where all errors are presented as 90% confidence limits.

We now address a critical question, namely, is there sufficient uncertainty in the $N(\text{H I})$ and $N(\text{D I})$ measurements to reconcile the γ^2 Vel D/H abundance ratio with the general result observed in the local ISM or with the D/H derived in Paper I for the sight line to δ Ori A? Figure 9a shows with dotted and dashed lines the expected appearance the Ly α profile would have if our measurement of $N(\text{D I})$ is correct but the $N(\text{H I})$ were made high enough so that $D/H = 1.5 \times 10^{-5}$. In Figure 9, the dotted line represents the H I profile that would be needed for the most probable value for $N(\text{D I})$, while the dashed lines represent the 90% confidence limits. For comparison, we also show in Figure 9a the best-fitting H I profile (solid line) derived in the previous section for this particular observation. Figure 9b is an analogous plot with $N(\text{H I})$ forced to take on a value so that $D/H = 0.74 \times 10^{-5}$ as observed toward δ Ori A (Paper I). From Figure 9 it is clear that forcing $N(\text{H I})$ to make $D/H = 1.5 \times 10^{-5}$, assuming $N(\text{D I})$ from §3.3, produces a very poor (and unacceptable) fit to the H I profile, and the fit becomes ridiculous if $D/H = 0.74 \times 10^{-5}$. We have assumed the best-fit continuum (solid line) to compute the Ly α profiles shown in Figure 9. We have also explored whether or not the D/H ratios can be reconciled by

Table 6. Abundance Ratios^a

	γ^2 Vel	ζ Pup	δ Ori A
$N(\text{D I})$ (10^{15} cm^{-2})	$1.12^{+0.15}_{-0.12}$	$1.30^{+0.19}_{-0.17}$	$1.16^{+0.29}_{-0.20}$
$N(\text{N I})$ (10^{15} cm^{-2})	4.10 ± 0.34	7.62 ± 0.84	6.19 ± 0.51
$N(\text{H I})$ (10^{19} cm^{-2})	5.13 ± 0.50	9.18 ± 0.89	$15.6 \pm 1.52^{\text{b}}$
D/H (10^{-5})	$2.18^{+0.36}_{-0.31}$	$1.42^{+0.25}_{-0.23}$	$0.74^{+0.20^{\text{b}}}_{-0.15}$
N/H (10^{-5})	7.99 ± 1.02	8.30 ± 1.22	3.97 ± 0.51
D/N	0.27 ± 0.04	0.17 ± 0.03	0.19 ± 0.05

^aAll errors presented in this table are 90% confidence limits (1.65σ).

^bErrors in $N(\text{H I})$ for δ Ori A from Paper I were revised to reflect the fact that potential systematic effects in $N(\text{H I})$ identified in this paper for ζ Pup may dominate the statistical errors quoted in the earlier paper. The 1σ error in $N(\text{H I})$ was set to 0.0256 dex. The errors in D/H for δ Ori A are essentially the same as found in Paper I since they are dominated by the errors in $N(\text{D I})$.

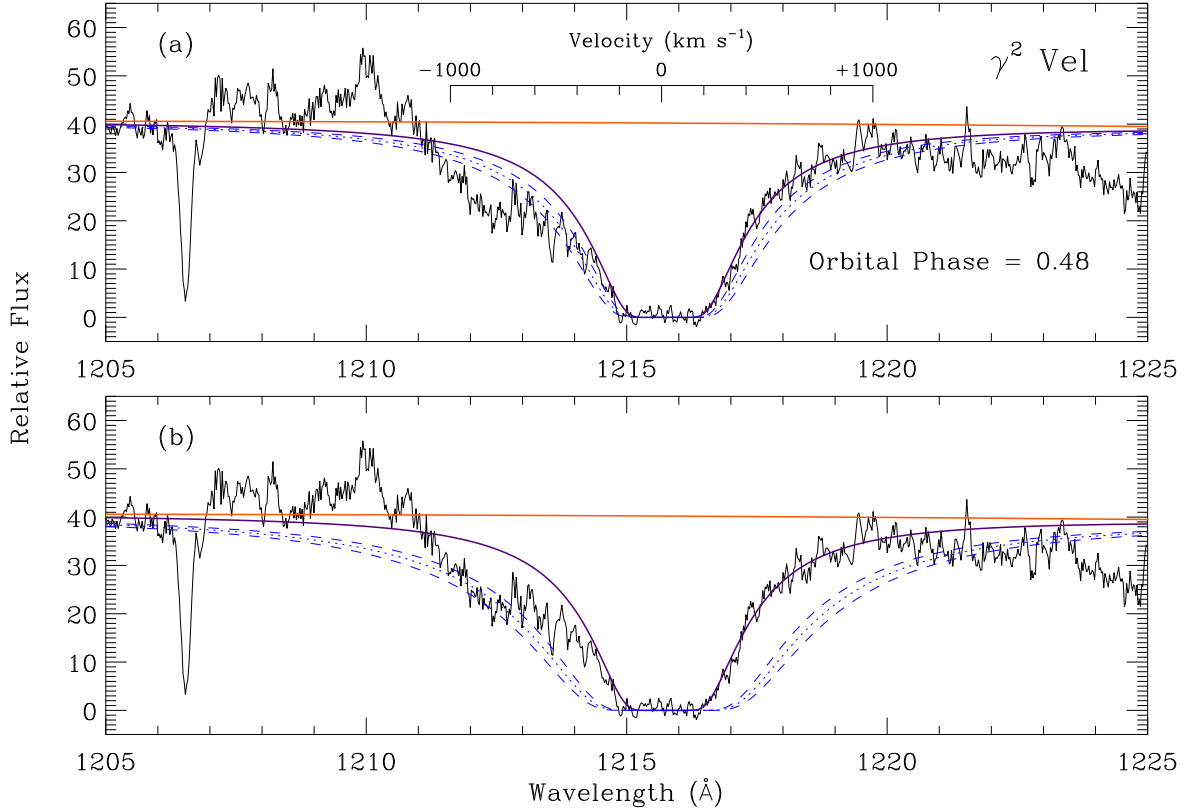


Fig. 9.— Expanded plots of the H I Ly α profile in γ^2 Vel shown in Figure 7b (SWP4719), again smoothed with a 5-pixel boxcar for display purposes only. The best-fitting profile and its corresponding continuum are indicated with solid lines. The broader damping profiles outside the best fit show the appearance of the profile when $N(\text{H I})$ is forced to take on a value so that (a) $\text{D}/\text{H} = 1.5 \times 10^{-5}$ as generally observed in the local ISM, given the values of $N(\text{D I})$ in Table 3 [the dotted line assumes the most probable $N(\text{D I})$ while the dashed lines use the 90% confidence limits on $N(\text{D I})$], and (b) $\text{D}/\text{H} = 0.74 \times 10^{-5}$ as observed toward δ Ori A in Paper I. Note that the region between 1207 and 1210 \AA is sometimes affected by P-Cygni emission (which happens to be weak in this observation, see Figure 7).

adjusting the continuum placement, and we found that absurd continuum placements and shapes must be assumed to make $D/H = 1.5 \times 10^{-5}$ or (even worse) 0.74×10^{-5} .

As demonstrated at the end of §3.3, the changes in $N(D\text{ I})$ needed to make $D/H = 1.5 \times 10^{-5}$ or 0.74×10^{-5} , assuming our most probable value of $N(H\text{ I})$, gave a large mismatch with the data, which were clearly unacceptable. We conclude that spatial inhomogeneities in D/H in the ISM within ~ 500 pc of the Sun have high statistical significance, especially when contrasting the D/H ratios in the directions of γ^2 Vel and δ Ori A, which were measured with the same instrument and techniques.

5.2. Nitrogen Abundances

The N I column density $N(N\text{ I})$ was computed by integrating the column density profiles shown in Figure 3. The $N(N\text{ I})$ results for the three targets are listed in Table 6. This table also contains the resulting N/H and D/N abundance ratios. We examined the potential error in $N(N\text{ I})$ by examining the errors in the portions of the various N I profiles used to construct $N_a(v)$. The 1σ uncertainty in $N(N\text{ I})$ for γ^2 Vel and δ Ori A is conservatively estimated to be 5% since the N I profiles were all of high quality. There may be some question about the structure in the core of $N_a(v)$ for ζ Pup. The uncertainty in $N(N\text{ I})$ for ζ Pup was estimated by supposing the spike in $N_a(v)$ at $v \sim 19$ km s $^{-1}$ is due largely to noise fluctuations in the core of N I $\lambda 952.5$, the weakest N I line we detect on this sightline. If we truncate the $N_a(v)$ profile at the level of the secondary maximum at $v \sim 24$ km s $^{-1}$ [$N_a(v) = 5.6 \times 10^{14}$ cm $^{-2}$ (km s $^{-1}$) $^{-1}$], we find that the area of the spike is 3.6×10^{14} cm $^{-2}$, or 4.7% of the total. We then suppose that the total uncertainty in $N(N\text{ I})$ for ζ Pup is $\sqrt{2}$ times this, or $1\sigma = 5.1 \times 10^{14}$ cm $^{-2}$, to allow for the possibility that there may be other such fluctuations.

6. DISCUSSION

There are two principal conclusions of the IMAPS D/H program. First, the atomic D/H ratio in the ISM, averaged over path lengths of 250 to 500 pc, exhibits significant spatial variability. Differences in the atomic D/H ratio on long pathlengths in the ISM have been suspected for many years (Vidal-Madjar et al. 1978; Vidal-Madjar & Gry 1984), but not until now have data of sufficient quality been available to evaluate and reduce statistical and systematic errors to levels where these differences are unequivocal. Second, we find no support for the simple picture that variations in D/H anticorrelate with those of N/H, i.e., one measure of how much the gas has been processed through stellar interiors. Figure 10 shows the relationship between D/H and N/H for the three sightlines studied by IMAPS plus the white dwarf G191–B2B (Vidal-Madjar et al. 1998; Sahu et al. 1999). We point out that some elements are systematically removed from the gas phase as they are incorporated into interstellar dust (Savage & Sembach 1996), but the abundance

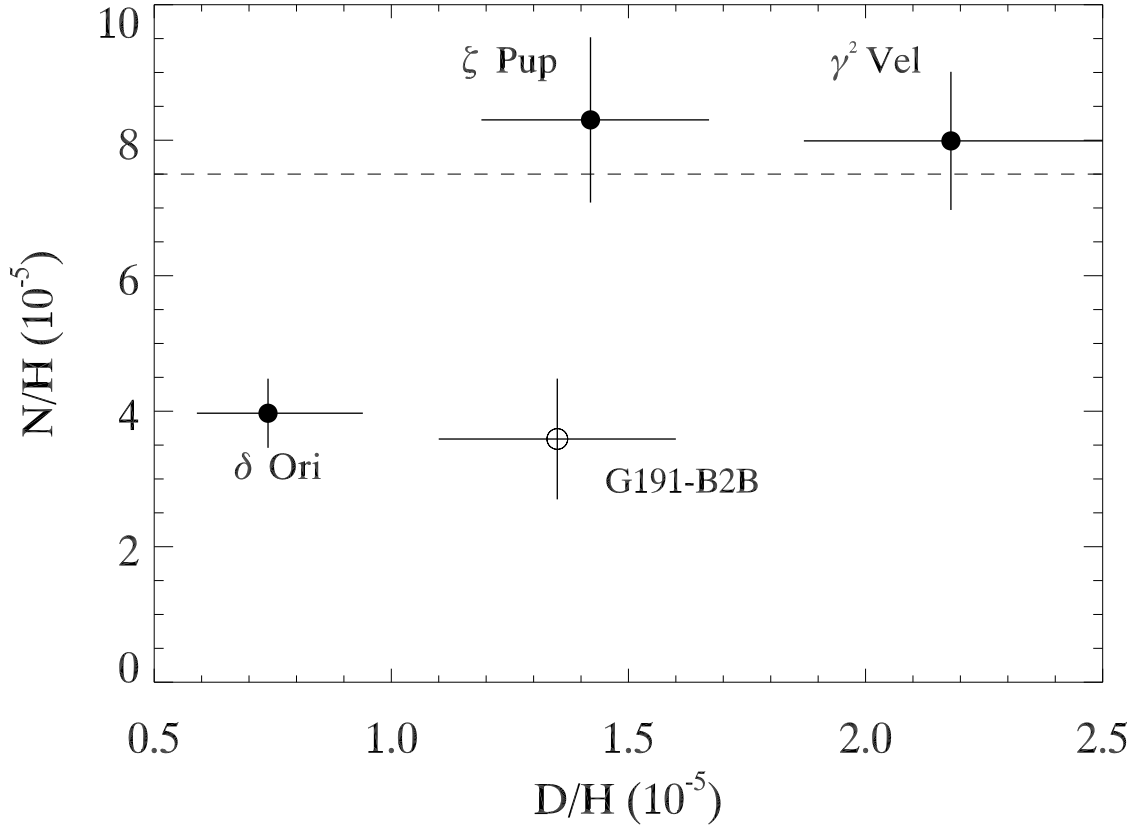


Fig. 10.— N/H abundance ratio as a function of D/H for the three stars studied by IMAPS plus the white dwarf G191-B2B. The abundance ratios for G191-B2B represent the full range of values reported by Vidal-Madjar et al. (1998) and Sahu et al. (1999). The average value of N/H in the ISM found by Meyer, Cardelli, & Sofia (1997) is indicated by a dashed line. The errors bars are 90% confidence limits (1.65σ).

of N does not seem to be appreciably altered by this effect (Meyer et al. 1997).

Beyond the effects from depletions onto dust, spatial variations in interstellar gas abundances can arise as a natural consequence of galactic chemical evolution and the changing influences of different stellar populations. The lack of an anticorrelation between N/H and D/H depicted in Fig. 10 indicates that the variability of D/H is not just a consequence of different mixing ratios of material with differing levels of stellar processing, as we might anticipate, for instance, from the variable addition of metal-poor, infalling gas from the Galactic halo (Meyer et al. 1994). We may need to go further and draw a distinction between contributions from stars that simply destroy deuterium and those that both destroy deuterium and enrich the medium with additional nitrogen. That is, we could envision some stars cycling material only through their shallow layers that are only hot enough to burn deuterium, while others eject material from much deeper layers where the synthesis of heavier elements has taken place. This additional level of complexity could explain the behavior that we observed.

Global models of Galactic chemical evolution (Audouze & Tinsley 1974; Tosi 1988a,b; Dearborn, Steigman & Tosi 1996; Scully et al. 1996; Tosi et al. 1998) describe the destruction of D during stellar formation, evolution, and eventual mass loss. These models predict variations in D/H, N, and O abundances that are manifested as abundance gradients on a scale of $\gtrsim 1$ kpc. However, the predicted trends in galactic abundances may not accurately represent what is observable in the diffuse ISM. Tenorio-Tagle (1996) showed that the chemical enrichment of the diffuse ISM by OB associations, including supernovae from massive stars, is a slow process. Following a supernova explosion, chemically enriched ejecta remain clumpy and not well mixed with the diffuse ISM it encounters until it is incorporated into new star forming regions. This is a result of very long time scales for diffusion between different parcels of gas in the warm (10^4K) and cold (10^2K) phases of the ISM.

The diffusion time scale for enriched gas to thoroughly mix with the warm diffuse ISM can be very long ($t_D > 10^{10}$ yr - Tenorio-Tagle 1996). On the spatial scale sampled by the IMAPS observations, different sight lines may encounter regions with very different dynamical and chemical histories. Differential galactic rotation and random cloud motions are expected to stir the diffuse ISM and chemically enriched parcels of gas, but these parcels retain their distinct chemical properties until they are disrupted through photoevaporation, most likely by the formation of new massive stars. Tenorio-Tagle finds that diffusion is efficient only for the hot phase of the ISM ($t_D < 10^6$ yr), which accounts for a very small fraction of the total diffuse ISM. Only after the enriched gas and diffuse gas are highly ionized would the chemically enriched gas from the earlier generation of stars quickly diffuse into the ambient ISM. Thus, the time scale for mixing interstellar gases with different processing histories can be much longer than the chemical evolution time scale. However, it is possible that interstellar turbulence and its secondary phenomena may accelerate the mixing rate. Since the distribution of star forming regions (OB associations) shows large inhomogeneities on scales $\lesssim 1$ kpc, their corresponding chemical enrichment of the ISM may be expected to be nonuniform as well. This is perhaps revealed indirectly by variations

in H II region abundances (Peimbert 1999) and solar-type stars at similar galactocentric radii (Edvardsson, et al. 1993).

Several processes unrelated to stellar nucleosynthesis may, under the right circumstances, alter the atomic D/H ratio of some parcels of interstellar gas (see Lemoine et al. 1999 for a review). D may be incorporated into HD (Watson 1973), but the fraction of molecular gas on our sight lines is very low (see Paper I). Differential radiation pressure on D and H (Vidal-Madjar et al. 1978; Bruston et al. 1981) may lead to a separation of D in some clouds near strong radiation fields. Adsorption of D onto dust grains (Jura 1982) may deplete D from the gas phase. Bauschlicher (1998) found that reactions of H and D with polycyclic aromatic hydrocarbon (PAH) cations might systematically provide some D enrichment in PAHs. A very different perspective has been offered by Mullan & Linsky (1999), who suggested that significant quantities of D may be formed in stellar flares from M dwarf stars and ejected into interstellar space. Some or all of these processes could be at work in the diffuse ISM and alter the atomic D/H ratio on individual sight lines, independent of the degree of chemical enrichment from stellar evolution. However, they have not yet been demonstrated to be quantitatively significant. Observational and theoretical tests of the efficiency and applicability of these processes are needed to better understand the mechanisms affecting the D/H ratio in the diffuse ISM.

While the D/H ratios derived from IMAPS spectra are in the general range expected from galactic chemical evolution models, a factor of three variation in the mean D/H ratio on path lengths of several hundred pc is unexpected. The apparent lack of an anti-correlation of the D/H abundance ratio with the metallicity of the gas and its variability on smaller than expected scales suggests that other processes in the Galaxy may be masking more general chemical evolution trends. This may pose a problem for deriving a “primordial” D/H by extrapolating back from D/H measurements in the Milky Way to extragalactic absorbers at higher and higher redshifts, or to even to evaluate “primordial” D/H directly from high redshift observations, until we understand the reasons for these differences. The spatial variations found in this study underline the importance of high-quality D/H determinations. D/H measurements in more distant regions of the Galaxy are needed to determine whether the properties of the gas within 500 pc of the Sun are representative of the Galactic disk. Observations with the FUSE satellite should probe such more distant environments and hopefully answer some of these questions.

The value of D/H for γ^2 Vel is larger than that usually considered typical for the Milky Way. This robust result establishes a new lower limit to the primordial D/H ratio. Within the framework of standard Big Bang Nucleosynthesis (Walker et al. 1991), the large value of D/H found toward γ^2 Vel is equivalent to a cosmic baryon density of $\Omega_B h^2 = 0.023 \pm 0.002$. This error simply reflects the uncertainty in the D/H ratio toward γ^2 Vel reported in this paper. We regard this value of $\Omega_B h^2$ as an upper limit since no correction has been applied for the destruction of deuterium in stars. This upper limit on $\Omega_B h^2$ is consistent with the preferred values of $\Omega_B h^2$ derived from recent analyses of the BOOMERANG and MAXIMA cosmic microwave background measurements (e.g., Lange et al. 2000; Tegmark & Zaldarriaga 2000; Hu et al. 2000). However, any lowering of

this upper limit on $\Omega_B h^2$ to correct for astration will lead to a marginal disagreement with simple inflation models (see Figure 4 in Tegmark & Zaldarriaga 2000) and requires adjustments of other cosmological parameters. Alternatively, the $\Omega_B h^2$ upper limit from D/H may be taken as a prior assumption for the constraint of other cosmological parameters using the CMB data (e.g., see Hu et al. 2000).

We wish to thank the US and German space agencies, NASA and DARA, for their joint support of the *ORFEUS-SPAS II* mission that made these observations possible. The successful execution of our observations was the product of efforts over many years by engineering teams at Princeton University Observatory, Ball Aerospace Systems Group, and Daimler-Benz Aerospace. Important contributions to the success of IMAPS also came from the efforts of D. A. Content and R. A. Keski-Kuha and other members of the Optics Branch of the NASA Goddard Space Flight Center and from O. H. Siegmund and S. R. Jelinsky at the Berkeley Space Sciences Laboratory. We also thank Bruce Draine for insightful discussions on atomic interactions with dust grains and PAHs. This work was supported in part by NASA grant NAG5-616 to Princeton University. The *IUE* data were obtained from the National Space Science Data Center at NASA-Goddard.

REFERENCES

- Anders, E., & Grevesse, N. 1989, *Geochim. Cosmochim. Acta*, 53, 197
- Audouze, J., & Tinsley, B. 1974, *ApJ*, 192, 487
- Bauschlicher, C. W. 1998, *ApJ*, 509, L125
- Bevington, P. R., & Robinson, D. K. 1992, *Data Reduction and Error Analysis for the Physical Sciences*, 2nd ed. (New York: McGraw Hill)
- Bianchi, L., & Bohlin, R. C. 1984, *A&A*, 134, 31
- Bluhm, H., Marggraf, O., de Boer, K. S., Richter, P., & Heber, U. 1999, *A&A*, 352, 287
- Boesgaard, A. M., & Steigman, G. 1985, *ARAA*, 23, 319
- Bohlin, R. C., Savage, B. D., & Drake, J. F. 1978, *ApJ*, 224, 132
- Bruston, P., Audouze, J., Vidal-Madjar, A., & Laurent, C. 1981, *ApJ*, 243, 161
- Dearborn, D. S. P., Steigman, G., & Tosi, M. 1996, *ApJ*, 465, 887
- Diplas, A., & Savage, B. D. 1994, *ApJS*, 93, 211
- Edvardsson, B., Anderson, J., Gustafsson, B., Lambert, D. L., Nissen, P. E., Tomkin, J. 1993, *A&A*, 275, 101
- Epstein, R. L., Latimer, J., & Schramm, D. N. 1976, *Nature*, 263, 198
- Ferlet, R. 1981, *A&A*, 98, L1
- Fitzpatrick, E. L., & Spitzer, L. 1994, *ApJ*, 427, 232

- Goldbach, C., Lüdtke, T., Martin, M., & Nollez, G. 1992, *A&A*, 266, 605
- Gölz, M., et al. 1998, in *Proc. IAU Colloq. No. 166, The Local Bubble and Beyond*, eds. D. Breitschwerdt, M. J. Freyberg, J. Trümper (Berlin: Springer), 75
- Hoffleit, D. & Jaschek, C. 1982, *The Bright Star Catalogue*, 4th ed., (New Haven: Yale U. Obs.)
- Howarth, I. D., Prinja, R. K., & Massa, D. 1995, *ApJ*, 452, L65
- Howk, J. C., & Sembach, K. R. 2000, *AJ*, in press, astro-ph/9912388
- Hu., W., Fukugita, M., Zaldarriaga, M., & Tegmark, M. 2000, astro-ph/0006436
- Hurwitz, M., et al. 1998, *ApJ*, 500, L1
- Jenkins, E. B. 1971, *ApJ*, 169, 25
- Jenkins, E. B., & Peimbert, A. 1997, *ApJ*, 477, 265
- Jenkins, E. B., Joseph, C. L., Long, D., Zucchini, P. M., Carruthers, G. R., Bottema, M., & Delamere, W. A. 1988, in *UV Technology II*, ed. R. E. Huffman (Bellingham: International Society for Optical Engineering), 213
- Jenkins, E. B., Reale, M. A., Zucchini, P. M., & Sofia, U. J. 1996, *Ap&SS*, 239, 315
- Jenkins, E. B. et al., 2000, *ApJ Letters*, in press
- Jenkins, E.B., Tripp, T. M., Woźniak, P. R., Sofia, U. J., & Sonneborn, G. 1999a, *ApJ*, 520, 182 (Paper I)
- Jenkins, E. B., et al. 1999b, *BAAS*, 31, 942
- Jura, M., 1982, in *Advances in Ultraviolet Astronomy (NASA CP-2238)* ed. Y. Kondo (Greenbelt: NASA), 54
- Lampton, M., Margon, B., & Bowyer, S. 1976, *ApJ*, 208, 177
- Lange, A. E., et al. 2000, astro-ph/0005004
- Lemoine, M., et al. 1999, *New Astr.*, 4, 231
- Linsky, J. L. et al. 1993, *ApJ*, 402, 694
- Linsky, J. L., Diplas, A., Wood, B. E., Brown, A., Ayres, T. R., & Savage, B. D. 1995, *ApJ*, 451, 335
- Massa, D. et al. 1995, *ApJ*, 452, L53
- Massa, D., Van Steenberg, M. E., Oliverson, N., & Lawton, P. 1998, in *Ultraviolet Astrophysics Beyond the IUE Final Archive (ESA SP-413)*, ed. W. Wamsteker & R. Gonzalez Riestra (Noordwijk: ESA), 723
- Meyer, D. M., Cardelli, J. A., & Sofia, U. J. 1997, *ApJ*, 490, L103
- Meyer, D. M., Jura, M., Hawkins, I., & Cardelli, J. A. 1994, *ApJ*, 437, L59
- Moos, H. W., et al. 2000, *ApJ Letters*, in press

- Morton, D. C. 1978, *ApJ*, 222, 863
- Morton, D. C., & Bhavsar, S. P. 1979, *ApJ*, 228, 147
- Morton, D. C. & Dinerstein, H. L. 1976, *ApJ*, 204, 1
- Morton, D. C, & Underhill, A. B. 1977, *ApJS*, 33, 83
- Mullan, D. J., & Linsky, J. L. 1999, *ApJ*, 511, 502
- Peimbert, M. 1999, in *Chemical Evolution from Zero to High Redshift*, eds. J. R. Walsh & M. R. Rosa (Berlin: Springer), 30
- Press, W. H., et al. 1992, *Numerical Recipes in Fortran*, 2nd ed. (Cambridge: Cambridge Univ. Press)
- Prinja, R. K. et al. 1992, *ApJ*, 390, 266
- Puldrach, A. W. A., Kudritzki, R. P., Puls, J., Butler, K., & Hunsinger, J. 1994, *A&A*, 283, 525
- Reid, A. H. N., & Howarth, I. D. 1996, *A&A* 311, 616
- Rogerson, J. B., Spitzer, L., Drake, J. F., Dressler, K., Jenkins, E. B., Morton, D. C., & York, D. G. 1973, *ApJ*, L97
- Rogerson, J. B., & York, D. G. 1973, *ApJ*, 186, L95
- Sahu, M. S. 1992, Ph.D. Thesis, Univ. Groningen
- Sahu, M. S. et al. 1999, *ApJ*, 523, L159
- Savage, B. D. & Sembach, K. R. 1996, *ARAA*, 34, 279
- Schaerer, D., Schmutz, W., & Grenon, M. 1997, *ApJ*, 484, L153
- Schmutz, W. et al. 1997, *A&A*, 328, 219
- Scully, S. T., Cassé, M., Olive, K. A., Schramm, D. N., Truran, J., & Vangoini-Flam, E. 1996, *ApJ*, 462, 960
- Shull, J. M., & Van Steenberg, M. E. 1985, *ApJ*, 294, 599
- Sofia, U. J., & Jenkins, E. B. 1998, *ApJ*, 499, 951
- Strickland, D. J., & Lloyd, C. 1990, *Observatory*, 110, 1
- Tegmark, M., & Zaldarriaga, M. 2000, *astro-ph/0004393 v3*
- Tenorio-Tagle, G. 1996, *AJ*, 111, 1641
- Tosi, M. 1988a, *A&A*, 197, 33
- Tosi, M. 1988b, *A&A*, 197, 47
- Tosi, M., Steigman, G., Matteucci, F., & Chiappini, C. 1998, *ApJ*, 498, 226
- van der Hucht, K. A., Conti, P. S., Lundström, I., & Stenholm, B. 1981, *Space Sci. Rev.* 28, 307
- Vidal-Madjar, A. 2000, in *The Light Elements and Their Evolution*, eds. L. da Silva, M. Spite, & J. R. de Medeiros, A.S.P. Conf. Ser., in press

- Vidal-Madjar, A., & Gry, C. 1984, *A&A*, 138, 285
- Vidal-Madjar, A., Laurent, C., Bonnet, R. M., & York, D. G. 1977, *ApJ*, 211, 91
- Vidal-Madjar, A., Laurent, C., Bruston, P., & Audouze, J. 1978, *ApJ*, 223, 589
- Vidal-Madjar, A., et al. 1998, *A&A*, 338, 694
- Walker, T. P., Steigman, G., Schramm, D. N., Olive, K. A., & Kang, H.-S. 1991, *ApJ*, 376, 51
- Watson, W. D., 1973, *ApJ*, 182, L73
- Welty, D. E., Morton, D. C., & Hobbs, L. M. 1996, *ApJS*, 106, 533
- York, D. G., & Rogerson, J. B. 1976, *ApJ*, 203, 378
- York, D. G., Spitzer, L., Bohlin, R. C., Hill, J., Jenkins, E. B., Savage, B. D., & Snow, T. P. 1983, *ApJ*, 266, L55